AN IMPROVED CHARACTERIZATION OF THE MULTIAXIAL
FRACTURE STRENGTH OF EGCR-TYPE AGOT GRAPHITE

by

ENRIQUE SAMUEL GARIBAY

B.S., Kansas State University, 1981

A MASTER'S THESIS

submitted in partial fulfillment of the
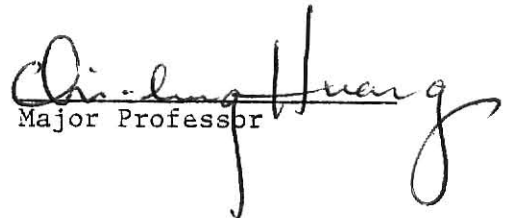
requirements for the degree

MASTER OF SCIENCE

Department of Mechanical Engineering

KANSAS STATE UNIVERSITY
Manhattan, Kansas

1983

Approved by:

Major Professor

THIS BOOK
CONTAINS
NUMEROUS PAGES
WITH THE ORIGINAL
PRINTING BEING
SKEWED
DIFFERENTLY FROM
THE TOP OF THE
PAGE TO THE
BOTTOM.

THIS IS AS RECEIVED
FROM THE
CUSTOMER.

ACKNOWLEDGEMENTS

TABLE OF CONTENTS

LIST OF TABLES

LIST OF FIGURES

CHAPTER I

INTRODUCTION

Brittle solid materials such as graphite are now being used in many

diverse applications in essentially all of industry. Graphite is being

used in metallurigical, chemical, electrical, nuclear, and mechanical

applications. When used in high temperature applications, the strength of

graphite has been found to increase with increasing temperature. Graphite

also has a high resistance to thermal shock. This is due to a combination

of high thermal conductivity and a low Young's Modulus. With it having

a high strength-to-weight ratio, graphite has become one of the leading

materials to be used in rockets and missles as unusual cone, nozzle, and

vane shapes. In nuclear applications, graphite is used as a moderator,

reflector, thermal column, and a shielding structure because of the in-

crease in strength and hardness when exposed to irradiation.

Prior to fracture, graphite has been found to exhibit a small amount

of plastic deformation. Like most other brittle materials, graphite is

compressible and has a higher strength in compression than in tension.

This is commonly referred to as the Bauschinger effect.

Graphite has a material symmetry unlike many other brittle materials.

The material properties in the plane perpendicular to the direction of

extrusion are considered to be invariant. Such a plane is called the iso-

tropic plane. The material properties in the isotropic plane, are, however,

quite different than the properties along the direction of extrusion. The

material symmetry so described is called transverse isotropy.

The broadening applications of graphite demonstrate that it is indeed a versatile industrial material. In order to take full advantage of its versatility, it is first necessary to characterize the fracture strength of the material under a combined state of stress. This is done by obtaining the fracture strength for any state of stress. In this thesis, the fracture strength is studied in the Compression-Compression, Compression-Tension, and Tension-Compression quadrants of biaxial stress.

Fracture strength data for EGCR-type grade-AGOT graphite was found by conducting uniaxial and biaxial tests at room temperature. Uniaxial tensile tests were conducted in the hoop and axial stress directions using "dog-bone" shaped test specimens. Biaxial fracture tests were conducted using the "pressure vessel" method. Thin-walled cylinders were subjected to a combination of inside pressure, outside pressure, and an axial load.

Finding the true fracture strength of brittle materials can often be complicated and difficult. The biaxial specimen geometry may have inherent stress concentrations that could possibly initiate failure. Also, local failure of the test specimen may initiate cracks which then propogate throughout the test specimen. Other complications arise when the ends of the test specimen are fixed or bonded which results in nonuniform stress distributions throughout the test specimen. When thin-walled cylinders are used in biaxial tests, it is necessary to choose an optimum specimen geometry which will be resistant to tubular buckling while maintaining a uniform stress distribution throughout the wall thickness.

Once fracture data has been obtained, it is then necessary to correlate the data to one of many failure criteria which have been proposed for brittle materials. For a triaxial state of stress, there are generally

six non-trivial components of stress which make up the stress tensor. A triaxial criterion is a set of equations which, if satisfied by the stress components, imply fracture. This criterion may be written as:

$$f(\sigma_k) = 1 \quad , \quad k = 1, \ldots, 6 \tag{1}$$

where σ_k is the contracted notation of the stress tensor. Equation (1) represents a failure surface in six-dimensional stress space. Failure is said to occur if the stress point is on the surface.

Fracture strength data obtained in this investigation seem to better characterize the failure surface of EGCR-type grade-AGOT graphite than the one by the previous investigator (19). The biaxial fracture strength values along the 45° diagonal in the Compression-Tension and Tension-Compression quadrants show an increased improvement over values obtained in a previous investigation and can now be used to provide a better fit of the fracture data to the proposed biaxial failure surface.

CHAPTER II

LITERATURE REVIEW

Introduction

Throughout the years, many investigators have attempted to character-
ize the fracture strengths of such solid brittle materials as graphite.
While there are those that are emperical, other failure criteria have been
based on the micro-mechanics of the material. Regardless of the basis for
the failure criteria, the criteria should be able to predict failure in
all states of stress.

A literature review of failure theories for brittle solids, uniaxial
investigations, and biaxial investigations has been conducted and the re-
sults are described hereafter. The type of material tested along with the
specimen geometry and orientation have also been described.

Triaxial Failure Theories for a Brittle Solid

Tang (42), in his excellent literature review of proposed failure
theories for brittle solids, describes the necessary and desirable require-
ments for a failure criterion of graphite. He requires that the criterion
be a scalar function so as to ensure its validity in all coordinate systems.
In order to ensure that the material strength is finite in all directions,
the failure surface must be closed, smooth, and convexed. The proposed
failure criterion must also include the Bauschinger effect, i.e. it must

-4-

account for graphite having a higher strength in compression than in tension. Other requirements involve consideration of the material symmetry in a transversely isotropic material along with a dependence on the hydrostatic state of stress. In addition, Tang states that the failure criterion should not only be able to predict failure in all states of stress, but it should be relatively simple and require a minimum amount of data to verify.

With the preceeding ground rules established, Tang (42) reviewed the four basic failure criteria which are hereafter presented and discussed. The four basic failure criteria are: 1) the maximum stress (strain) theory, 2) the maximum shear stress theory, 3) the maximum strain energy theory, and 4) the maximum distortion energy theory.

1) <u>Maximum Normal Stress (Strain) Criterion</u>. The maximum normal stress criterion is one of the simplest and most widely used failure criterion as it applies well to brittle materials. The criterion postulates that failure occurs when the maximum normal stress at a point reaches a critical value regardless of the other stresses. The maximum normal stress criterion takes into account the Bauschinger effect. This is done by simply assigning two values for ultimate strength; one value for tension and the other for compression. In biaxial tension, the maximum normal stress criterion tends to overestimate the strength of graphite because the principal stresses are not aligned with the material axes.

The maximum normal strain criterion postulates that material failure is controlled by a limiting tensile strain. This criterion would imply higher strengths in biaxial tension than in uniaxial tension which Price (41) found not to be true for graphite.

Tang (42) found the maximum normal stress (strain) failure criterion to be deficient in several areas and therefore, not applicable to graphite. It was found deficient because it represents a multi-segmented failure surface rather than a smooth surface. Also, the criterion is expressed in terms of the three principal stress components rather than the six which are needed when the material axes and the principal stress axes do not coincide.

2) <u>Maximum</u> <u>Shear</u> <u>Stress</u> <u>Criterion</u>. The maximum shear stress criterion postulates that during yielding of a ductile material, slippage occurs along critically oriented planes. Material slippage suggests that the maximum shearing stress plays a key role in failure. Tresca (44) postulated that yielding of a ductile material depends only on the maximum shearing stress that is attained within an element, i.e. the shear strength of the material. Coulomb (6) and Mohr (33) postulated that the shear strength of a brittle material depends on the cohesive strength of the material and the coefficient of internal friction on the fracture plane. Because the criterion is expressed by a linear equation of major and minor principal stresses, it is easy to see how the Bauschinger effect may be accounted for. Although the Coulomb-Mohr theory has been widely accepted, Tang (42) felt it had unrealistic assumptions and implications. It fails to predict failure where the maximum tensile stress reaches a critical value before shear stress does. It also implies that the failure criterion is independent of the intermediate principal stress.

In his work, Paul (35, 36, 37) addressed these deficiencies. His criterion approximated a non-linear curved fracture surface in three dimensional principal stress space by a multi-segmented linear surface. Tang

does not recommend this criterion for graphite applications because it fails
to represent a smooth failure surface.

3) <u>Maximum Strain Energy Criterion</u>. The maximum strain energy criter-
ion postulates that brittle fracture occurs when the elastic strain energy
reaches a critical value. Ely (10) modified this criterion for a trans-
versely isotropic material under a biaxial state of stress when he inter-
preted his biaxial data of graphite. In his modification, Ely allowed for
more than one independent strength parameter. In doing so, each of the two
principal stresses was normalized by the appropriate tensile or compressive
strength for the same principal stress direction. Tang commented that this
failure criterion was good for biaxial loading but may not be as good for
triaxial loading because it represents a multi-segmented fracture surface
in the principal stress plane.

4) <u>Maximum Distortion Energy Criterion</u>. Von Mises' maximum distor-
tion energy theory (32) is based on energy concepts in an effort to predict
the plastic yielding of ductile materials that are isotropic, incompressible,
and free of the Bauschinger effect. Von Mises postulated that failure of a
ductile material occurs when the strain energy of distortion reaches a
certain limit (characteristic of the material).

Grassi and Cornet (15), Fisher (13), and Coffin (5) considered the
Bauschinger effect in their theories developed specifically for gray cast
iron. Their applications to graphite are considered to be limited because
they represent a multi-segmented failure surface. Hoffman (21) also modi-
fied Von Mises' theory. In his criterion, Hoffman included effects of all
six stress components, but did not account for dependence on the hydrostatic
state of stress.

In review, all the previously mentioned failure criteria fail to contain any higher ordered terms of stress other than the quadratic. The failure criteria are restricted to the case where the reference axes are coincident with the material axes. This implies that the criteria are not applicable to alternate coordinate systems. The failure criteria also fail to include all interactions of the six stress components.

In light of the many shortcomings of the four basic failure criteria, the theory developed by Tsai and Wu (45) seems to be the best available failure theory for graphite applications. Their theory is a failure theory of polynomial form which should be valid for any anisotropic brittle solid exhibiting the Bauschinger effect. Because this criterion considered only second order terms, it is relatively easy to characterize experimentally.

A strength criterion for anisotropic materials was proposed by Gol'denblat and Kopnov (14). It is in polynomial form and is known as the strength tensor theory. This theory takes into account the Bauschinger effect and the influence of stress interaction. In their work, Gol'denblat and Kopnov (14) only considered the case of orthotropic plane stress, while Tsai and Wu's work (45) gave quadratic forms of the strength function explicitly for orthotropic materials. Based upon the work of Gol'denblat and Kopnov (14), Huang (22,23) generated the invariants of the stress tensor for each of the crystal classes from consideration of invariant transformations of the strength function. By these invariants, the strength function can be expressed as a general polynomial form higher than the second order. Merkle (31) used a special case of Tsai and Wu's theory when he proposed an ellipsoidal yield criterion for a compressible transversely isotropic graphite.

A quadratic polynomial failure theory for a transversely isotropic material can be written as:

$$F_1(\sigma_1 + \sigma_2) + F_3\sigma_3 + F_{11}(\sigma_1{}^2 + \sigma_2{}^2 + 2\sigma_6{}^2) + F_{33}\sigma_3{}^2$$
$$+ F_{44}(\sigma_4{}^2 + \sigma_5{}^2) + 2F_{12}(\sigma_1\sigma_2 - \sigma_6{}^2) + 2F_{13}(\sigma_1\sigma_3 + \sigma_2\sigma_3) = 1 \tag{2}$$

where the strength constants F_1, F_3, F_{11}, F_{33}, F_{44}, F_{12}, and F_{13}, respectively, are the seven independent strength tensor components for a transversely isotropic material. Equation (2) was written with reference to the material axes such that X_3 is the axis coincident with the axis of extrusion as shown in Figure 1.

Uniaxial Investigations

Greenstreet et al. (16) investigated the mechanical properties of EGCR-type AGOT-graphite. In that investigation, data was obtained from tests performed at room temperature, 1000°F, 2000°F, and 4500°F with the majority of the testing done at room temperature. Uniaxial tests were conducted using three different specimen orientations. Two had their longitudinal axes perpendicular to the direction of extrusion and to each other. The third was aligned so that the longitudinal axis was parallel to the direction of extrusion. Specimens of each orientation were used to test in compression and tension. In order to study size effects including volume and cross-sectional area, various geometries were used in uniaxial tension and compression. It was found that size effects were small or nonexistent within the size range investigated (5/8 in.-3/8 in. diameter). It was also concluded that the behavior of AGOT graphite was the same in felxural and in
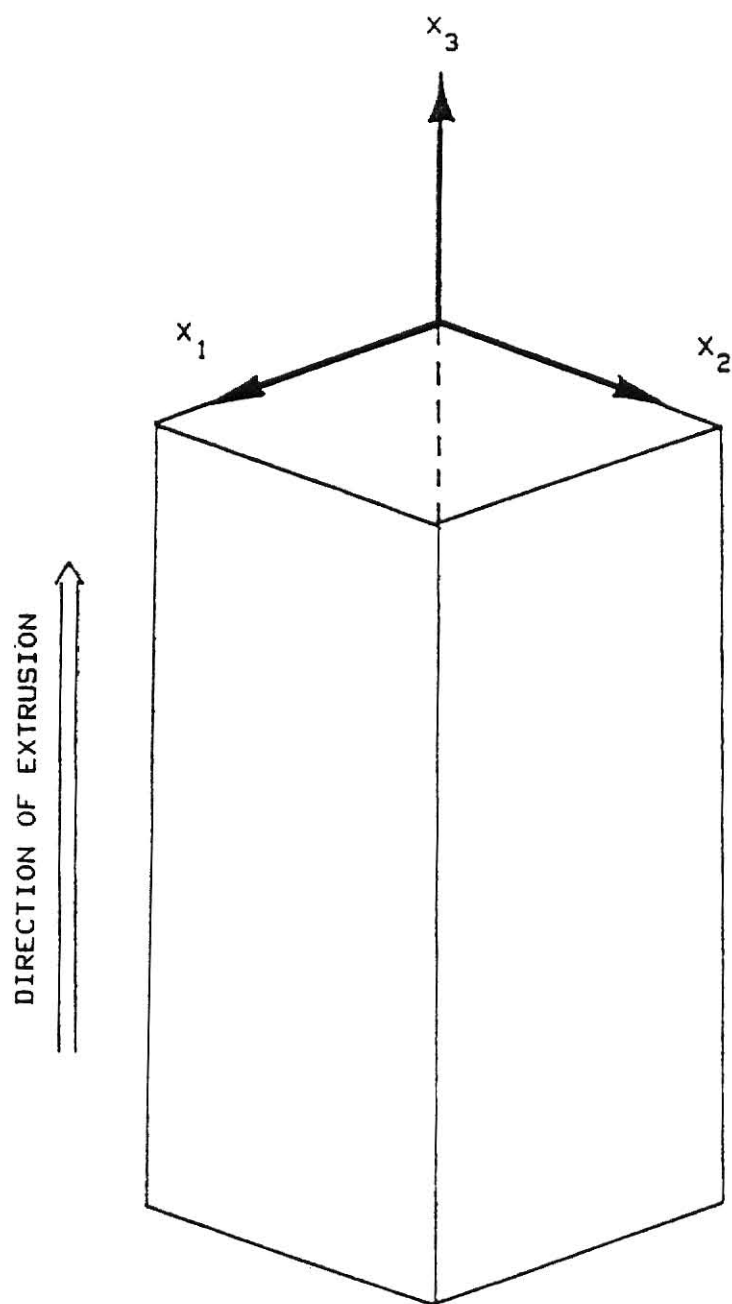
Figure 1: Material Axes of Extruded Graphite

uniaxial tests. Uniaxial values of strength reported by Greenstreet were
based on averages of data obtained from several specimen geometries. In
the parallel direction, tensile and compressive strengths were reported as
1570 psi and 4800 psi, respectively. Tensile and compressive strength
values reported in the transverse direction were 930 psi and 4930 psi, re-
spectively.

In his work with Chelmsford granite, Peng (38) found that the uniaxial
compressive strength of the granite can vary anywhere from 14,000 psi to
30,000 psi, depending on the type of inserts used between the specimen and
the loading platens. Peng (39) later examined rock and steel specimens to
determine the elastic deformation of the cylindrical specimens. Test speci-
mens used in that investigation were 1.25 in. in diameter and had a L/D
ratio of 2.0. The cylindrical test specimens were subjected to the following
end conditions: perfect confinement, direct contact, uniform loading,
teflon inserts, and neoprene inserts. It was concluded that highly non-
uniform stress distributions are developed under end conditions of perfect
confinement. Peng also concluded that the more expansive the end-inserts,
the more non-uniform are the stress distributions throughout the test speci-
mens.

Off-axis uniaxial tension and compression tests were performed by
Jortner (26,27) on ATJ-S graphite. Uniaxial test specimens for tension
and compression tests were oriented at angles of 0°, 30°, 45°, and 90° to
the direction of extrusion. Specimens used in uniaxial tensile tests had
gage diameters of 0.25 in. and gage lengths of 2.0 in. Overall length of
the tensile specimens was 6.0 in. Specimens used in uniaxial compression
tests had gage diameters of 0.5 in. and gage lengths of 0.5 in. In his
investigation, Jortner stated that "available evidence suggests that

compression failure of ATJ-S graphite takes place by shear at an angle approximately 45° to the loading axis."

A small-deformation elastic-plastic continuum theory used to describe the stress-strain behavior of Graphitite-G was examined by Greenstreet et al. (18). Uniaxial tensile tests were performed at room temperature using two separate specimen geometries. With-grain tensile specimens used gage diameters of 0.31 in. and a gage length of 0.75 in. The overall length of the tensile specimen was 5 in. Against-grain tensile specimens used gage diameters of 0.125 in. and a gage length 0.5 in. with an overall length of 1.75 in. In that investigation, Greenstreet et al. concluded that cycling of uniaxial tensile specimens had no apparent influence on failure.

Other investigations of graphite include Taylor et al. (43) and Marshall et al. (30). Taylor et al. studied the mechanical properties of three types of isotropic reactor graphites with and without fast neutron irradiation at 150°C in DIDO. Solid cylinders were used to measure uniaxial tensile and compressive strengths. In that study, they found that tensile and shear strengths of graphite increased with neutron irradiation. Marshall et al. studied American Poco Graphite and used experimental data and the Weibull method to compare predictions of graphite strength under tensile and bending loads using fracture mechanics.

In his review of experimental procedures, Tang (42) describes a bi-axial test program developed by Ho (20) to test graphite. In that test program, Ho describes the recommended geometries for uniaxial tension and compression tests. The tensile specimen is described by a 0.75 in. gage diameter and a gage length of 2.5 in. The compression specimen recommended by Ho has a diameter of 0.5 in. and a length of 1.5 in.

The standard methods of testing carbon and graphite mechanical materials in tension and compression are covered in the ASTM standards C565-78 and C695-81, respectively. Uniaxial tensile tests require a specimen with a gage diameter of 0.31 in. and a total length of 5 in. A recommended height to diameter ratio of 2.0 is given for compression specimens. For further details on specimen geometry, see appendix.

The Industrial Graphite Engineering Handbook (46) lists average compressive strengths of graphite at room temperature. The handbook notes that the compressive (as well as tensile) strength of graphite increases with increasing temperature. Nightingale (34) also noted this strength characteristic of graphite. In the book, Nuclear Graphite, Nightingale (34) reports the compressive strength of AGOT graphite to be 6000 psi in both the parallel and transverse directions.

Biaxial Investigations

Within the last fifteen years, many experimental investigations have been performed in an effort to find fracture strengths of graphite materials. The majority of the investigations have been conducted at room temperature while a few investigations have performed tests at elevated temperatures. The majority of biaxial data has been obtained by testing thin-wall tubular specimens subjected to internal, external, and axial pressures. Biaxial test specimens were manufactured such that their longitudinal axis was coincident with the direction of extrusion.

Weng (50), in a thorough study of ATJ graphite, confirmed the general belief that low strength values of graphite in the compression-compression quadrant are primarily due to the arch action of the thin-walled tube

specimens under biaxial compression. From this, Tang (42) concluded that because of premature buckling of the tubular specimens, existing biaxial compression data should not be used to verify failure theories.

Jortner (25) conducted biaxial fracture tests on POCO AXF-5Q graphite. Tests were conducted in the tension-tension (T-T) and tension-compression (T-C) quadrants at 70°F, 3000°F, and 4000°F. Jortner found that the failure surface at an elevated temperature was similar to the failure surface at room temperature but displaced to a higher level of stress.

Broutman et al. (2) also used tubular specimens of POCO AXM-5Q graphite to test in the T-T and T-C quadrants. They found that their tests results were better characterized by Ely's failure theory in the T-C quadrant, while data in the T-T quadrant could be characterized by a cross between Mohr and Ely's failure theories.

Taylor et al. (43) performed an extensive study of three types of isotropic reactor graphites with and without fast neutron irradiation at 150°C in DIDO. In that study, solid cylinder specimens were exposed to hydrostatic pressure and axial compression. From the results, they concluded that tensile and shear strengths increased with neutron irradiation.

Babcock et al. (1) used a tubular geometry to perform biaxial fracture tests on ATJ-S graphite. Tests were conducted at elevated temperatures in the C-C, T-T, and C-T quadrants. From the data, they concluded that ATJ-S graphite showed very low anisotropy.

Extensive biaxial tests on Graph-I-tite Grades A and G graphite were performed by Ely (7,8,11). To test in the T-T and T-C quadrants, Ely (8) used tubular test specimens with threaded ends. Each test specimen had a wall thickness of 0.06 in., a gage length of 3.5 in., and a I.D. of 1.0 in. Ely noted the "time-to-fracture" for all tests (time duration of the

biaxial test) and found that values of strength were not significantly altered by a rate change as small as those reported. Ely noted a 9 percent increase in the mean strength of graphite when the "time-to-fracture" rate was increased by a factor of 25.

Ely, in a separate investigation of Graph-I-tite graphite (9), used two types of tubular test specimens. Ely employed the same long tube geometry as was used before (8) when testing in the T-C and T-T quadrants. For C-C and T-C tests, Ely used a short tube geometry which had a wall thickness of 0.063 in., a total length of 1.25 in., and an I.D. of 1.187 in.

A later investigation of Graph-I-tite graphite was performed by Ely (12). In that study, biaxial tests were performed in all stress quadrants using specimen gage lengths of 1 in., 2 in., and 3 in. All test specimens had a wall thickness of 0.075 in. and a I.D. of 1.19 in. Ely concluded that the specimen gage length was a critical parameter for the pressure vessel test method. The largest C-C strengths were obtained using a specimen gage length of 1 in. Ely noted that T-T and T-C tests were not as dependent on gage length as were C-C tests.

Similar biaxial tests were conducted by Weng (47,48,49,50) but on Grades ATJ and JTA graphite. Greenstreet et al. (17) conducted biaxial tests of RAXM support element graphite using tubular geometries. Testing was performed in the T-T and T-C quadrants. Uniaxial and biaxial fracture data of H327 graphite were obtained by Cobb, Parry, and Engle (4) and also by Price and Cobb (40).

Jortner tested ATJ-S graphite at room temperature and at 2000°F (26,27). All biaxial test specimens were subjected to low strain rates. A long and short tubular specimen geometry was used in the testing. The long and short tubular geometries employed a wall thickness of 0.05 in., gage lengths

of 1 in. and 0.8 in., an I.D. of 1.01 in., and total lengths of 4 in. and
3.15 in., respectively. Jortner conducted a buckling analysis (27) on his
biaxial test specimen using a standard MDAC-West computer program designed
to make a stability analysis of orthotropic cylinders under an axial load
and lateral pressure. Results of the buckling analysis indicate that tubu-
lar buckling may be experienced when axial compressive stresses greater
than 6000 psi and tangential compressive stresses greater than 3800 psi are
attained.

Greenstreet et al. (18) used thin-walled cylinders to obtain data on
the loading and unloading response of Graph-I-tite graphite. Test speci-
mens were loaded by internal pressure only. Cylindrical test specimens had
a wall thickness of 0.092 in., a gage length of 6 in., and a mean radius of
0.922 in. The nonlinear stress-strain behavior of graphite under combined
stress at room temperature was found to be accurately described by a small-
deformation elastic-plastic continuum theory.

To date, there are no standards governing the biaxial testing of
brittle materials. In his review of experimental procedures, Tang (42)
credits Ho (20) as providing the best biaxial test plan of brittle materials.
In his investigation of ATJ-S graphite (28), Jortner states that "The tri-
axial test can be a versatile tool for experimentally studying both defor-
mational and incremental constitutive laws. Further test work in an improved
facility, capable of precise (automated) proportional load-path control,
would undoubtedly provide useful results."

CHAPTER III

MATERIALS AND TEST PROCEDURES

Introduction

Tests conducted on EGCR-type AGOT graphite consisted of uniaxial ten-
sile tests employing "dog-bone" shaped specimens, and biaxial fracture
tests using thin-walled hollow cylinders. Uniaxial tensile tests were
conducted in the hoop and axial directions such that their longitudinal
axes were either perpendicular or parallel to the parent billet direction
of extrusion. Biaxial fracture tests were conducted such that the specimen
longitudinal axis was parallel with the direction of extrusion.

Biaxial fracture tests were conducted using the "pressure vessel"
method. An optimized specimen geometry was chosen such that the test speci-
men would be more resistant to tubular buckling. This geometry employs a
short gage length and a reduced wall thickness which allows for use of the
thin-wall approximation in calculating hoop-stress.

Test procedures for uniaxial testing is described hereafter. Biaxial
fracture test procedures for each quadrant are also described. Pressure
regulators, pressure gages, and associated testing equipment and materials
used in this investigation were all salvage. It is, therefore, difficult to
provide specifications concerning the equipment and materials used herein.

Description of Material

The material tested in this investigation was EGCR-type grade-AGOT
graphite. Material was obtained from the Nuclear Engineering Department
at Kansas State University with no available documentation as to the origin
of the graphite. Specimens used in the investigation were taken from ex-
truded billets of size 4-3/8 X 4-3/8 X 51 in. Maximum particle size of
the graphite was 1/32 in. while being of 99.9 percent carbon with a density
of 1.72 g/cc.

As is the case of transversely isotropic materials, each element has
an axis of material symmetry. For an extruded material such as AGOT, the
direction of the axis of symmetry coincides with the extrusion direction,
which is called the "parallel" direction. The direction normal to this
axis is called the "transverse" direction. Material properties along the
parallel direction are different from those along the transverse direction.

All tests in this investigation were done at room temperature. Four
uniaxial tensile specimens were oriented such that their longitudinal axes
were parallel to the direction of extrusion, while a second set of three
was oriented in the transverse direction. All biaxial test specimens had
their longitudinal axes parallel to the direction of extrusion.

Uniaxial tensile tests were conducted using "dog-bone" shaped test
specimens. The specimen taper was used to ensure failure at the gage sec-
tion and to reduce any Poisson effects acting at the cylinder ends. The
cylindirical specimens had a gage diameter of 3/4 in. and a overall length
of 3 in.

The biaxial test specimens used in this and the previous investigation
(19) are shown in Figure 2. Cylinder dimensions were chosen with a D/T
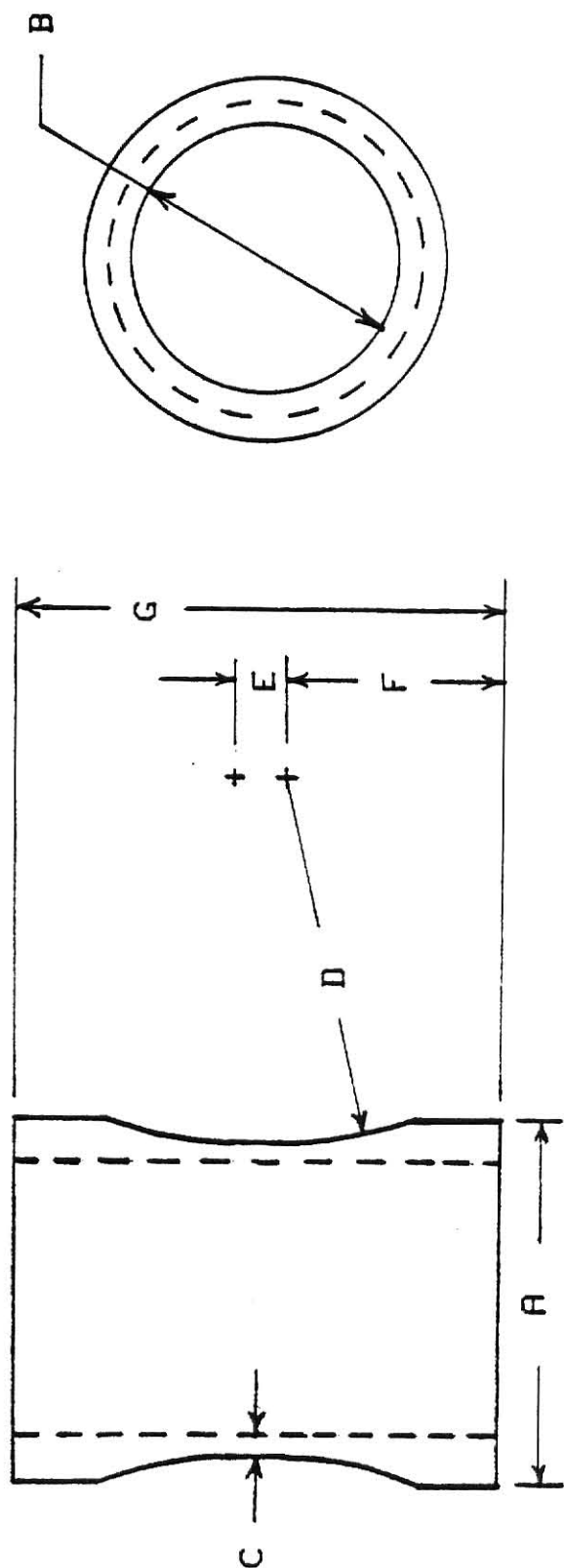
A	B	C	D	E	F	G
3.75	2.75	0.20	3.75	0.50	2.25	5.00
3.75*	2.75*	0.25*	2.50*	1.00*	2.50*	5.00*

*As used by Hackerott (19)

Figure 2:   Biaxial Test Specimen Geometries (inches)

(Diameter/Wall Thickness) ratio of 15.75 and a L_g/t (gage length/wall thickness) ratio of 2.5, while ratios used in the previous investigation were 13.0 and 4.0, respectively. Considerations in choosing the tube geometry were such that a larger D/T ratio should be used that will yield a thinner wall. In doing so, a uniform stress distribution may be assumed throughout the wall thickness. The L_g/t ratio is also an important parameter. By reducing the gage length, there is less chance of tubular buckling. The transition from the outside gage diameter to the outside cylinder diameter (the "neck-down" area) is designed to minimize the effect of Poisson's ratio and any stress concentrations that may exist at the cylinder ends. This also helps ensure that failure will occur at the gage section.

Description of Uniaxial Tension Test Apparatus and Procedure

The uniaxial tensile test apparatus is shown in Figure 3. The apparatus consists of two end caps made of 2024-T6 aluminum which were machined and drilled in the same operation to ensure proper alignment of the 7/16 in. NF studs inserted into the ends. It was important that the load be applied through the centerline of the specimen so as to avoid any bending moments which might give extraneous results. Attached to the studs are 1/8 in. diameter stranded stainless steel cables which are used to transmit the tensile load. A Riehle 20,000-pound test machine was used to apply the uniaxial tensile loads.

Test preparation for uniaxial tensile tests consisted of visually inspecting the cylinder surface to detect any surface flaws that might exist. If the specimen was free of surface flaws, the gage diameter was recorded. The specimen and the end caps were then wiped clean of any graphite powder
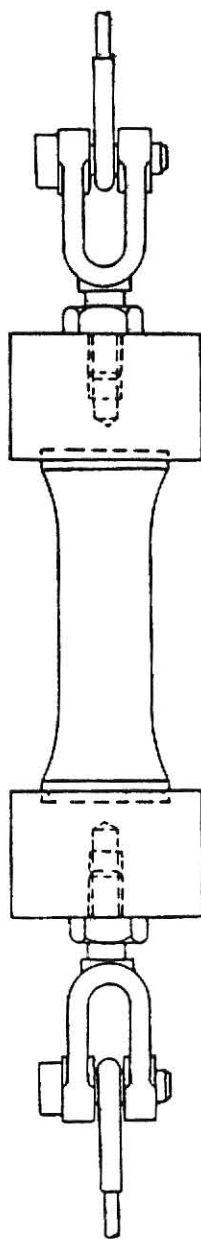
Figure 3: Uniaxial Tensile Test Apparatus

to insure a good adhesive bond. The end caps were bonded to the test speci-
men using Sikadur 31 Hi-Mod Gel adhesive. Adhesive was applied to the ends
of the specimen and to the end caps. End caps and specimen were then assem-
bled and placed in a lathe where they were allowed to rotate. The end caps
and specimen all rotated at different velocities. In doing so, any air
bubbles or voids in the adhesive were allowed to dissipate. This also
helped to ensure proper alignment between the specimen and end caps.

Description of Biaxial Test Apparatus

Biaxial tests on the graphite cylinders were conducted using the appa-
ratus shown in Figure 4. By pressurizing the stainless steel cylinder
through the various ports, different states of stress were imposed upon the
graphite. The stainless steel cylinder has an excellent inside surface fin-
ish because it was originally used as a hydraulic component. The cylinder
has a pressure rating of 5000 psi. The end platens were made of 2024-T6
aluminum with grooves cut for 1/8 in. neoprene o-rings which provided seals
between the test specimen and the end platens and between the end platens
and stainless steel cylinder.

The biaxial test specimens were pressurized using nitrogen gas as the
load medium as shown in the pressure schematic of Figure 5. It was chosen
over a hydraulic system primarily because of its cleanness. If there was
failure of the wax barrier which allowed gas to penetrate the graphite
cylinder, it was felt that gas would have less effect on the graphite than
would a fluid such as water. The system consisted of two gas regulators
which provided a constant pressure supply to the cylinder. Also included
were three pressure gauges, two of which read the output pressures of each

O-Rings

Teflon Gasket

Upper End Platen

Graphite Specimen

Lower End Platen

Spacer

Lock Ring
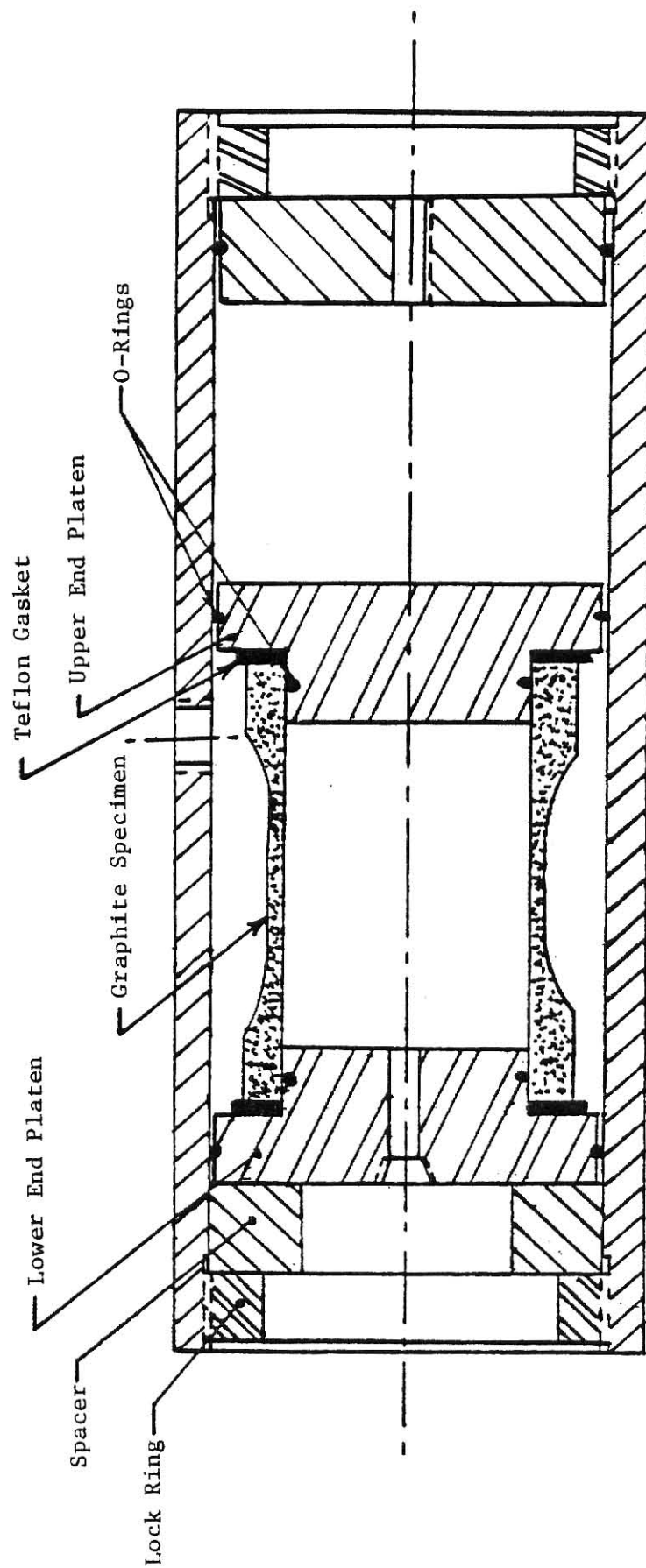
Figure 4: Assembled Biaxial Test Apparatus with C-C Test Specimen
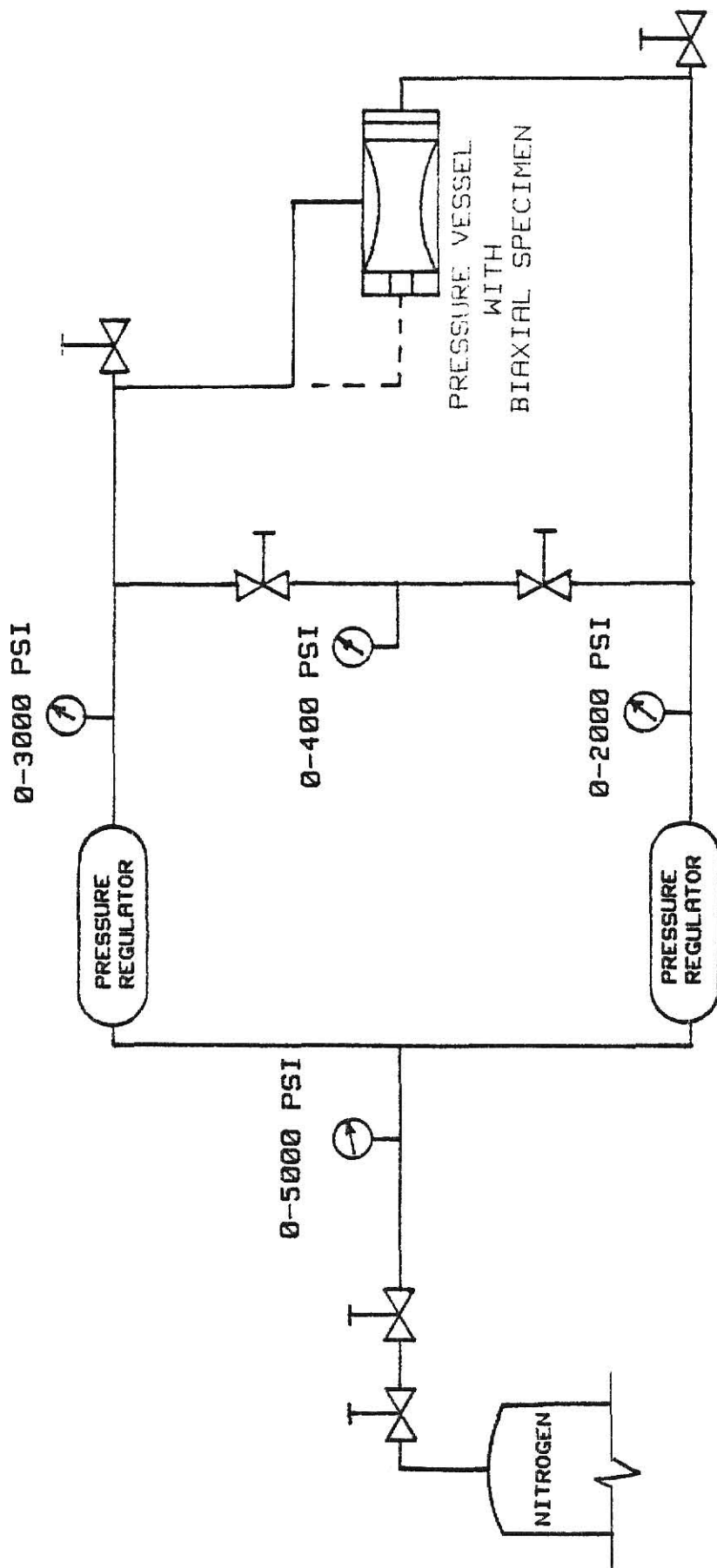
Figure 5: Pressure Schematic for Biaxial Testing

regulator. The third gauge had a lower pressure rating and was able to give more accurate measurements at lower pressures. It could be tied into either pressure channel by opening or closing the two valves shown.

Once a specimen had been pressurized to failure, the pressure in each channel fell drastically. If pressures were not immediately read, it was necessary to plug and repressurize the lines in order to read failure pressures. The pressure regulators were such that they would usually supply the same pressure as before once the source was reopened. It was standard practice by the investigator to record channel pressures as the test progressed so that incorrect pressures would not be reported.

Biaxial Test Procedures

Biaxial tests on graphite were conducted in three quadrants of the hoop-axial stress space. These quadrants were: 1) Compression-Compression (C-C), 2) Tension-Compression (T-C), and 3) Compression-Tension (C-T). Different states of stress were obtained by pressurizing the specimen through various ports on the stainless steel cylinder.

1) Compression-Compression Biaxial Test Procedures. Preparing for a Compression-Compression biaxial test consisted of first visually inspecting the cylinder surface to detect any surface flaws that might exist. If the cylinder was free of flaws, the inside and outside gage diameters were measured and recorded. These measurements were made in two places 90° apart at different axial locations.

Jortner (27) found that when gas pressures on the order of 1000 psi were applied to graphite, localized tensile stresses can initiate fracture. It is also known that when there is a 50 psi or greater pressure difference

across uncoated graphite cylinder walls, nitrogen gas will flow through the specimen walls. For these reasons, C-C specimens were coated with paraffin wax to provide a barrier. Paraffin wax was easy to apply and easy to clean off the ends. If the wax barrier cracked and allowed gas to pass through the walls, multiple dippings in hot wax corrected the problem. Paraffin wax also had a short setup time.

Slight pre-heating of the graphite cylinders was necessary when applying wax so that the wax would adhere to the cylinder walls. After multiple dippings were made, the wax was allowed to cool and the cylinder ends were scraped clean of wax. This was done in an effort to provide a flat surface between the graphite cylinder and the teflon pads.

Teflon pads were placed on the end platens during C-C tests. These were inserted to help alleviate any Poisson's effects at the cylinder ends. O-rings were placed between the inside cylinder wall and end platens and also between the end platens and the stainless steel cylinder wall. A thin coating of vacuum grease was applied to the o-rings to ensure a good seal. When assembling the test specimen to the end platens, a small steel cylinder was placed inside in order to alleviate any post-fracture damage to the test specimen. Once the stainless steel cylinder had been thoroughly cleaned, it was lubricated with motor oil to reduce friction. The test sample was then placed in the stainless steel cylinder and end caps inserted and secured.

Biaxial C-C tests required that the cylinder outside wall and top end platen be pressurized. Pressures were applied to these areas through the side and top ports respectively. Pressure on the outside cylinder wall provided the compressive hoop stress while pressure on the top platen provided the compressive axial stress.

Loading of C-C specimens followed a radial line in hoop-axial stress space. A typical incremental load path is shown in Figure 6, with the load path slope given as S_1. During the first half of the load path, large hoop and axial stress increments were used. These increments never exceeded 664 psi for hoop stress, and 275 psi for axial stress. In the second half of the load path, smaller increments were used. Near failure, hoop stress, and axial stress increments were on the order of 265 psi and 110 psi respectively. Channel pressures were recorded at time of failure.

2) <u>Tension-Compression</u>, <u>Compression-Tension Biaxial Test Procedures</u>. Visual inspection of all T-C, and C-T test samples was performed so that surface flaws might be detected. If the specimen was free of flaws, the inside and outside gage diameters were measured and recorded. These measurements were made at two places 90° from one another as was done in C-C tests. Specimens were then bonded directly to the end platens using Sikadur 31 Hi-Mod Gel adhesive. It should be noted that bonding yields different end conditions than those experienced with the use of teflon pads.

Biaxial C-T testing provides for pressurizing the cylinder outside wall and the top end platen. Biaxial T-C tests are attained by pressurizing the cylinder inside wall and the top end platen. Once the adhesive had cured, wax was applied to both the inside and outside walls of the test sample. Procedures in waxing were the same as those in C-C tests. All wax on end platens was removed and o-rings were inserted and greased. Again, the stainless steel cylinder was thoroughly cleaned and lubricated with motor oil in order to reduce friction. The test specimen was then inserted into the steel cylinder and end caps inserted and secured.

Loading of C-T, T-C specimens was similar to C-C tests inasmuch as it followed a radial line in hoop-axial stress space. Typical C-T, and T-C
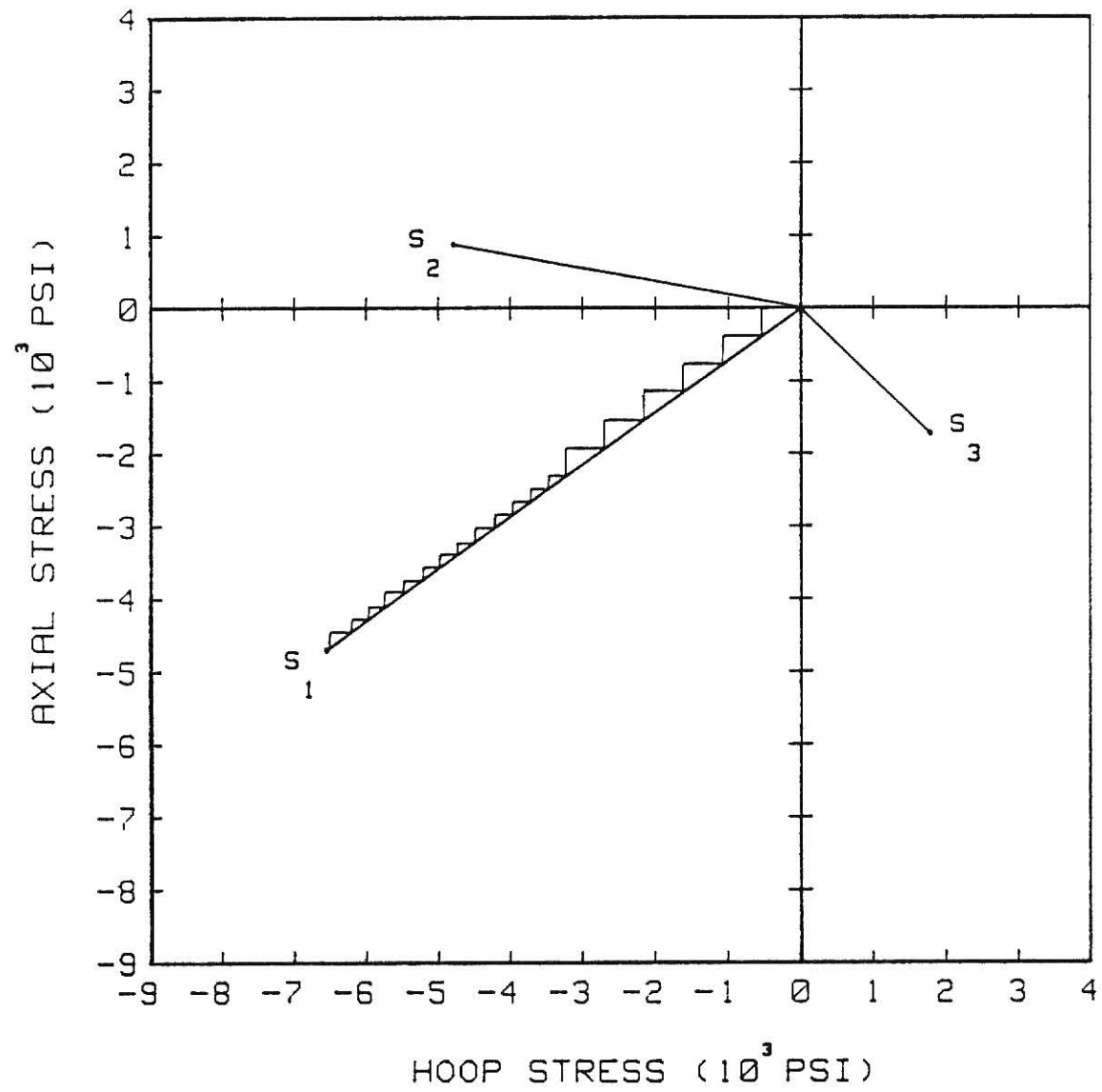
Figure 6:   Typical Incremental Load Paths Used in Biaxial Testing

load paths with slopes S_2, and S_3 respectively are shown in Figure 6. During the first half of the C-T load path, large hoop and axial stress increments were used. These increments never exceeded 1106 psi for hoop stress and 250 psi for axial stress. Near failure, the stress increments never exceeded 74 psi for hoop stress, and 45 psi for axial stress. Large stress increments were also used on the T-C tests. During the first half of the load path, hoop and axial stress increments did not exceed 148 psi. Near failure, both stress increments were on the order of 36 psi. Channel pressures were recorded at time of failure.

Calculation of hoop stress in this investigation, is based on the thin-wall approximation. This approximation assumes a uniform stress distribution throughout the cylinder wall thickness. The equations for calculating hoop and axial stress are as shown:

$$\sigma_H = \frac{(P_i - P_o)(d_o + d_i)}{2(d_o - d_i)} \tag{3}$$

$$\sigma_A = \frac{(P_o - P_t)d^2 - (P_o d_o^2 - P_i d_i^2)}{(d_o^2 - d_i^2)} \tag{4}$$

where

σ_H = hoop (transverse) stress

σ_A = axial (longitudinal) stress

P_o = pressure applied to the outside of the test specimen

P_i = pressure applied to the inside of the test specimen

P_t = pressure applied to the top of the end platen

d_o = outside diameter of test specimen gage section

d_i = inside diameter of the test specimen

d = 4.3778 in. = inside diameter of the stainless steel cylinder

In biaxial testing of graphite, the strength tensor, Equation (2), reduces to:

$$F_1\sigma_1 + F_3\sigma_3 + F_{11}\sigma_1^2 + F_{33}\sigma_3^2 + 2F_{13}\sigma_1\sigma_3 = 1 \qquad (5)$$

Strength components F_1, F_3, F_{11}, F_{33}, F_{13} are inherent material parameters which are to be determined experimentally by uniaxial and biaxial tests.

Let (X_t, Y_t, Z_t) = Tensile strengths in (X_1, X_2, X_3) directions, respectively.

Let (X_c, Y_c, Z_c) = Compressive strengths in (X_1, X_2, X_3) directions, respectively.

Note that for a transversely isotropic material, $X_t = Y_t$ and $X_c = Y_c$.

Also let $R_t(45^\circ)$ = Positive shearing strength in the plane of symmetry (X_1, X_3).

and let $R_c(45^\circ)$ = Negative shearing strength in the plane of symmetry (X_1, X_3).

With these values, Equation (5) yields:

$$F_1 = \frac{1}{X_t} - \frac{1}{X_c} \qquad\qquad F_3 = \frac{1}{Z_t} - \frac{1}{Z_c}$$

$$F_{11} = \frac{1}{X_t X_c} \qquad\qquad F_{33} = \frac{1}{Z_t Z_c} \qquad (6)$$

The strength component, F_{13}, may be evaluated by use of shear strength values (24) such that:

$$F_{13} = \frac{-1}{2}\left[\frac{1}{R_t(45^\circ)\,R_c(45^\circ)} - \frac{1}{Z_t Z_c} - \frac{1}{X_t X_c} \right] \qquad (7)$$

While Hackerott (19), calculated F_{13} from the relation:

$$F_{13} = \frac{1}{2\alpha B^2} \left[1 - B(\alpha F_1 + F_3) - B^2(\alpha^2 F_{11} + F_{33}) \right] \tag{8}$$

where σ_1 = hoop stress, σ_3 = axial stress, $\alpha = \sigma_1/\sigma_3$, and B is the value of σ_3 at failure.

CHAPTER IV

UNIAXIAL AND BIAXIAL FRACTURE TEST RESULTS AND DISCUSSION

Introduction

Results of experiments described in Chapter III are presented and dis-
cussed in this chapter. Data for uniaxial tensile strength tests and biaxial
fracture tests are given. These results are shown in hoop-axial stress space.
Data obtained by Hackerott (19) are also reproduced in the figure for pur-
poses of comparison. Typical failure modes are described for all tests.
A summary of test results is given at the end, along with values for uniaxial
and biaxial strengths. The independent strength components F_1, F_3, F_{11}, F_{33},
and F_{13}, have been calculated and are also given.

Uniaxial Tension Tests

Data from the uniaxial tensile tests are shown in Table 1. The data
table lists the specimen number, orientation of the specimen, gage diameter,
and fracture strengths for each test. Brief descriptions of failure modes
are also given. Uniaxial compression and tension strength results from
Hackerott (19) are included for purposes of comparison. All tensile
strength tests of this investigation were conducted using "dog-bone"
shaped specimens that were 3 in. in length. Fracture strengths were cal-
culated by dividing the applied tensile load by the cross-sectional area

Specimen Number*	Parent Billet Axis Parallel to Specimen Longitudinal Axis**	Gage Section Diameter (inches)	Specimen Length (inches)	Fracture Strength (psi)	Fracture Type***
		Compression			
A	X_1	0.997	2.5	5636	2
B	X_1	1.002	2.5	6151	4
C	X_1	1.001	2.0	5643	3
D	X_1	1.000	2.0	5989	2
E	X_2	1.000	2.5	5539	4
F	X_2	0.999	2.5	6137	5
G	X_3	1.002	2.0	6569	2
H	X_3	0.999	2.5	6328	6
J	X_3	0.946	2.5	5395	4
K	X_3	0.946	2.5	5976	2
L	X_3	1.002	2.5	5517	4
		Tension			
M	X_3	0.7535	2.75	2341	9
N	X_3	0.7515	2.75	1759	7
O	X_2	0.7509	2.75	1040	8
P	X_2	0.7520	2.75	1403	8
Q	X_1	0.7500	3.0	1188	8
R	X_1	0.7506	3.0	1148	8
S	X_1	07500	3.0	1365	8

Table 1: Uniaxial Compression and Tension Test Results

Specimen Number*	Parent Billet Axis Parallel to Specimen Longitudinal Axis**	Gage Section Diameter (inches)	Specimen Length (inches)	Fracture Strength (psi)	Fracture Type***
		Tension			
T	X_1	0.7500	3.0	994	8
U	X_3	0.7510	3.0	2678	10
V	X_3	0.7507	3.0	2377	10
W	X_3	0.7500	3.0	2370	8

*Test Results A-P are results reported by Hackerott (19).
**X_3 corresponds to the longitudinal axis of the billet.

***1. Longitudinal Cracks.
  2. Multiple cracks, longitudinal and angular.
  3. Fracture at edge of specimen end.
  4. Single crack at angle originating at edge of specimen end.
  5. Single crack not originating at edge of specimen end.
  6. No visible fracture.
  7. Fracture at adhesive bond.
  8. Perpendicular to longitudinal axis at transition between radius and gage section.
  9. Failure of fixture.
  10. Perpendicular to longitudinal axis within the gage section.

Table 1: Uniaxial Compression and Tension Test Results
(continued)

of the gage section using the nominal diameter of 0.75 in. Uniaxial data points are shown in hoop-axial stress space of Figures 7, 8, 11(a), and 11(b).

In the previous investigation, Hackerott (19) tested two uniaxial tensile specimens in the hoop stress direction. These two data points, O and P, had fracture strengths of 1040 and 1403 psi, respectively. In the present study, four uniaxial tensile fracture tests were conducted in the hoop stress direction. These tests were Q, R, S, and T. Fracture strengths were 1188, 1148, 1365, and 994 psi, respectively. With the exception of test T, all fracture strengths lie between those strengths reported by Hackerott and seem to typify the uniaxial fracture strength in the positive hoop stress direction.

Along with the two uniaxial tensile tests conducted in the hoop stress direction, Hackerott (19) also tested two uniaxial specimens in the positive axial stress direction. These were tests M and N which had fracture strengths of 2341 and 1759 psi, respectively. In the present study, three uniaxial tests were U, V, and W. The fracture strengths of these tests were 2678, 2377, and 2370 psi, respectively. These three uniaxial tests yielded larger fracture strengths than those reported in the previous investigation (19) and seem to better characterize the fracture strength in the positive axial stress direction.

Failure of uniaxial tensile specimens usually occurred at the transition between the gage section and the "neck-down" section of the test specimen. This typical tensile failure is shown in Figure 9. Failure planes were perpendicular to the longitudinal axis of the specimen. This indicates pure tensile failure. Failure at the gage section ends may indicate a region of high stress concentration.
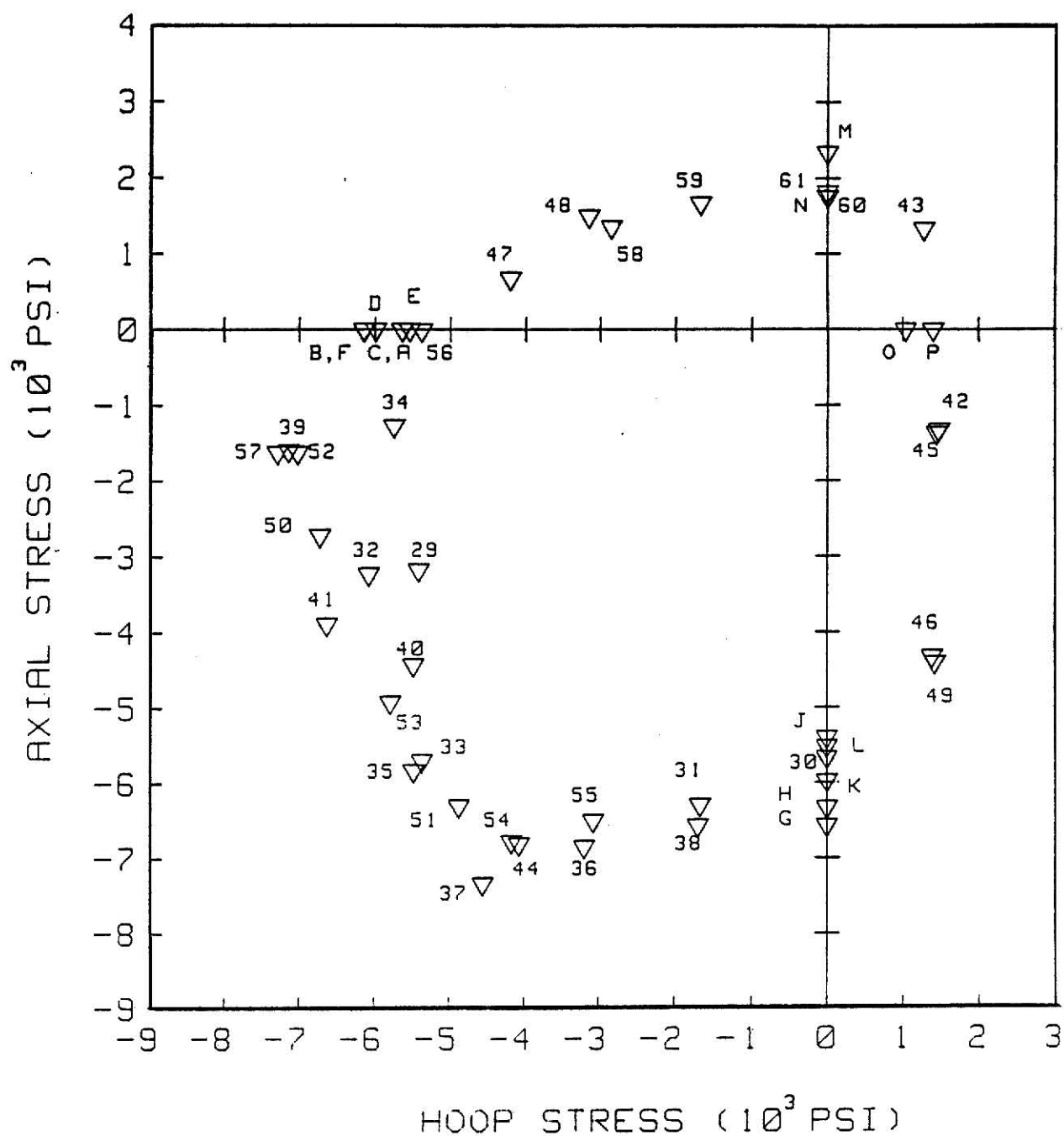
Figure 7:   Fracture Strengths for AGOT Graphite
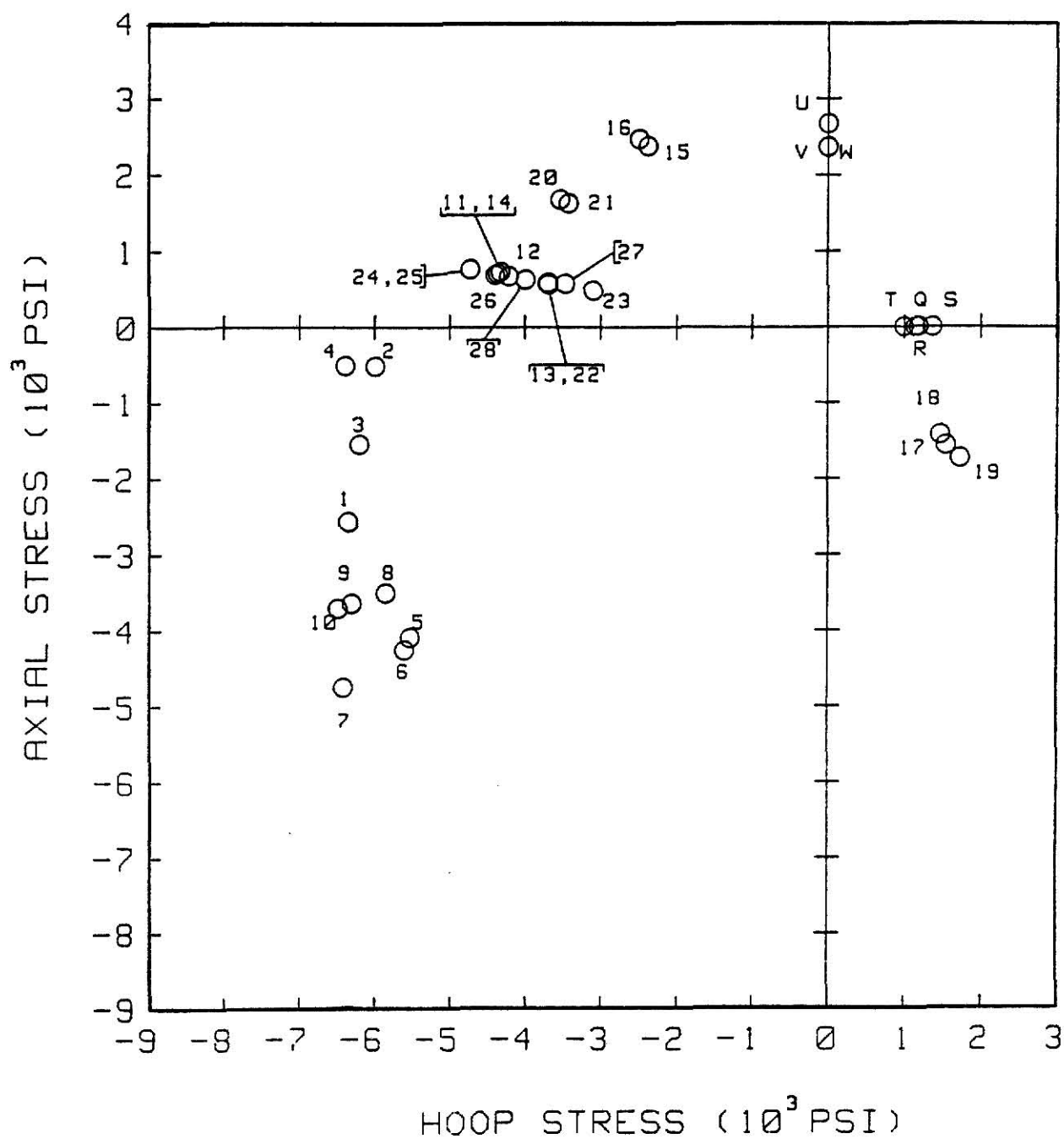from Hackerott (19)

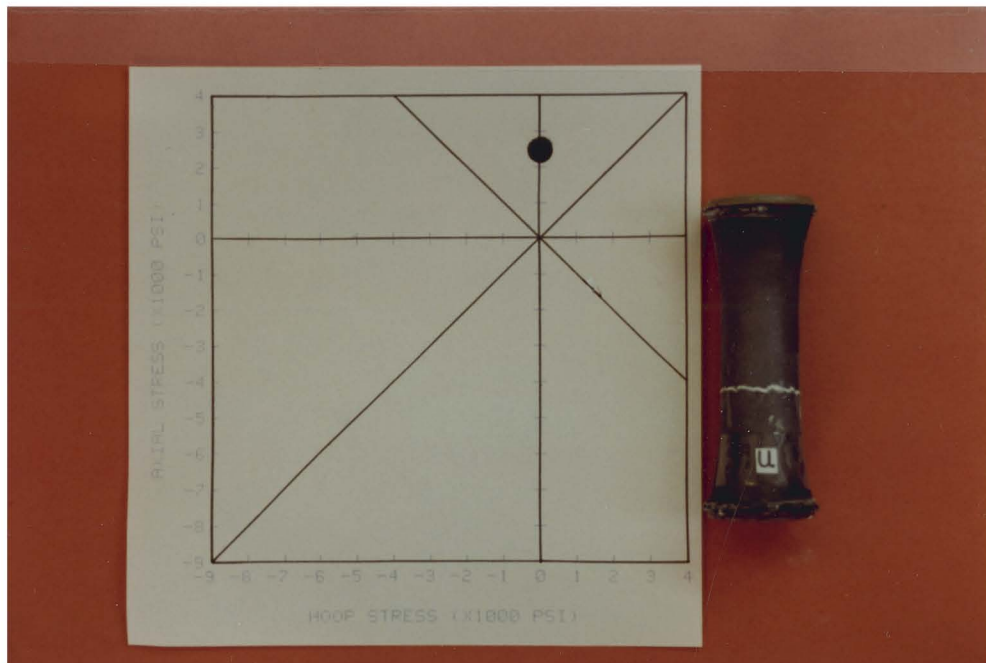Figure 8: Fracture Strengths for AGOT Graphite

Figure 9: A Uniaxial Tensile Specimen After Failure

Uniaxial tensile specimens used in this investigation have a different L/D ratio from that used in the previous investigation (19). The L/D ratio used in this investigation was 4, while Hackerott used a ratio of 3. ASTM Standard C565-78 calls for a L/D ratio of 16 when tensile testing graphite (appendix). Greenstreet et al. (16) used two sizes of uniaxial tensile specimens in their testing of EGCR-type AGOT graphite. Large specimens had gage diameters of 5/8 in. and gage lengths of 3 in., while the small specimens had gage diameters of 5/16 in. and gage lengths of 1-1/2 in. Specimen geometry used in this investigation was limited by the Riehle test machine. Had the test specimen been longer, the total length of the test specimen and the attached cables would have been too long to fit in the test machine.

Small surface flaws on the graphite uniaxial tensile specimens seemed to have little effect on the fracture strength of the graphite. Even though small flaws existed on the surface of the gage section, failure seldom occurred at these flaws. Knibbs (29) believed that failure of graphite was initiated by grains containing incipient cracks whose lengths were equal to the size of the coke particle.

In order to procure more reliable uniaxial tensile data, it is felt that a new specimen geometry should be chosen that will have a larger L/D ratio than that used in this investigation. Special attention should be given to the amount of adhesive applied to the specimen ends. If adhesive is applied along the sides of the specimen as well as at the ends, resulting failures may not be pure tensile in nature. They may in fact result in shear failure as was observed in a few tensile specimens not reported herein due to the inhomogeneous stress field.

More reliable uniaxial tensile data may also be obtained by performing flexure tests on graphite specimens. Greenstreet et al. (16) found that graphite behaved the same in flexure and in uniaxial tests, and that the stress-strain diagrams do not differ in an engineering sense. ASTM Standard D790M-81 provides for three and four-point testing of brittle materials. Beam theory is used to find the tensile stress on the outermost edge of the graphite area tested. The calculated tensile stress is only valid for materials that have linear stress-strain curves. The fact that graphite does not exhibit a linear stress-strain curve will, hence, introduce an error when calculating the tensile stress. Besides, the stress gradient on tensile strength cannot be ignored.

Biaxial Fracture Tests

Data from the biaxial fracture tests are shown in Table 2. Included in the table are values of hoop and axial stress at failure, inside and outside diameters, and the type of fracture sustained by each specimen. For purposes of comparision, biaxial fracture data of Hackerott (19) are also included.

Fracture of the biaxial test specimens was explosive. There was no forewarning as to when failure might occur. Because of the testing method and apparatus, there was no way to see where failure of the cylinder had been initiated. Typical failure modes for each stress quadrant are shown in Figures 10(a), 10(b), and 10(c).

1) <u>Compression-Compression</u> Tests. Biaxial C-C data is shown in hoop-axial stress space in Figures 7, 8, 11(a), and 11(b). Data obtained by Hackerott (19), in the lower portion of C-C quadrant, seemed to adequately

Specimen Number*	Hoop Stress (psi)	Axial Stress (psi)	Inside** Diameter (inches)	Outside** Diameter (inches)	Fracture Types***
1	-6343	-2560	---	----	1
2	-5989	-515	2.7506 2.7509	3.1538 3.1537	1
3	-6195	-1542	2.7498 2.7494	3.1527 3.1525	2
4	-6387	-506	2.7540 2.7531	3.1546 3.1546	2
5	-5531	-4087	2.7552 2.7561	3.1541 3.1548	2,4
6	-5605	-4251	2.7533 2.7547	3.1546 3.1548	2,4
7	-6416	-4738	2.7527 2.7523	3.1573 3.1572	2,4
8	-5856	-3501	2.7513 2.7506	3.1514 3.1514	2,4
9	-6306	-3635	2.7500 2.7500	3.1535 3.1535	2,4
10	-6490	-3700	2.7519 2.7520	3.1558 3.1556	2,4
11	-4314	732	2.7524 2.7512	3.1531 3.1531	6
12	-4204	673	2.7520 2.7514	3.1517 3.1515	6
13	-3688	561	2.7503 2.7500	3.1525 3.1525	6
14	-4388	690	2.7544 2.7547	3.1540 3.1543	6
15	-2390	2380	2.7507 2.7506	3.1530 3.1528	6

Table 2: Biaxial Test Results

Specimen Number*	Hoop Stress (psi)	Axial Stress (psi)	Inside** Diameter (inches)	Outside** Diameter (inches)	Fracture Types***
16	-2508	2471	2.7532 2.7530	3.1538 3.1538	6
17	1549	-1560	2.7525 2.7522	3.1537 3.1536	1
18	1475	-1422	2.7523 2.7522	3.1537 3.1534	1
19	1733	-1732	2.7519 2.7521	3.1529 3.1526	3,4,5
20	-3540	1685	2.7536 2.7512	3.1569 3.1550	6
21	-3429	1634	2.7542 2.7523	3.1555 3.1550	6
22	-3688	594	2.7525 2.7529	3.1531 3.1530	6
23	-3098	484	2.7517 2.7515	3.1527 3.1528	6
24	-4720	769	2.7494 2.7510	3.1542 3.1540	5
25	-4720	769	2.7527 2.7526	3.1539 3.1536	5
26	-4351	711	2.7539 2.7539	3.1548 3.1546	6
27	-3466	574	2.7495 2.7505	3.1509 3.1508	6
28	-3983	629	2.7506 2.7507	3.1498 3.1502	6
29	-5410	-3174			
30	0	-5665			
31	-1665	-6294			

Table 2: Biaxial Test Results (continued)

Specimen Number*	Hoop Stress (psi)	Axial Stress (psi)	Specimen Number*	Hoop Stress (psi)	Axial Stress (psi)
32	-6071	-3227	49	1424	-4408
33	-5362	-5691	50	-6719	-2719
34	-5741	-1266	51	-4868	-6300
35	-5470	-5828	52	-7017	-1620
36	-3193	-6846	53	-5782	-4916
37	-4548	-7335	54	-4167	-6775
38	-1692	-6569	55	-3072	-6499
39	-7137	-1592	56	-5379	-11
40	-5480	-4422	57	-7288	-1620
41	-6625	-3886	58	-2855	1355
42	1472	-1332	59	-1671	1667
43	1280	1328	60	0	1753
44	-4065	-6807	61	0	1823
45	1442	-1371			
46	1388	-4327			
47	-4207	670			
48	-3155	1497			

*Test results 29-61 are results reported by Hackerott (19)
**Measurements made 90° apart at different axial locations
***1. Excessive post fracture damage made initial fracture type indiscernible.
    2. Gage section broken into small fragments.
    3. Fracture at ends of gage section.
    4. Full length longitudinal crack
    5. Failure close to adhesive
    6. Single Circumferential crack at the transition of gage section.
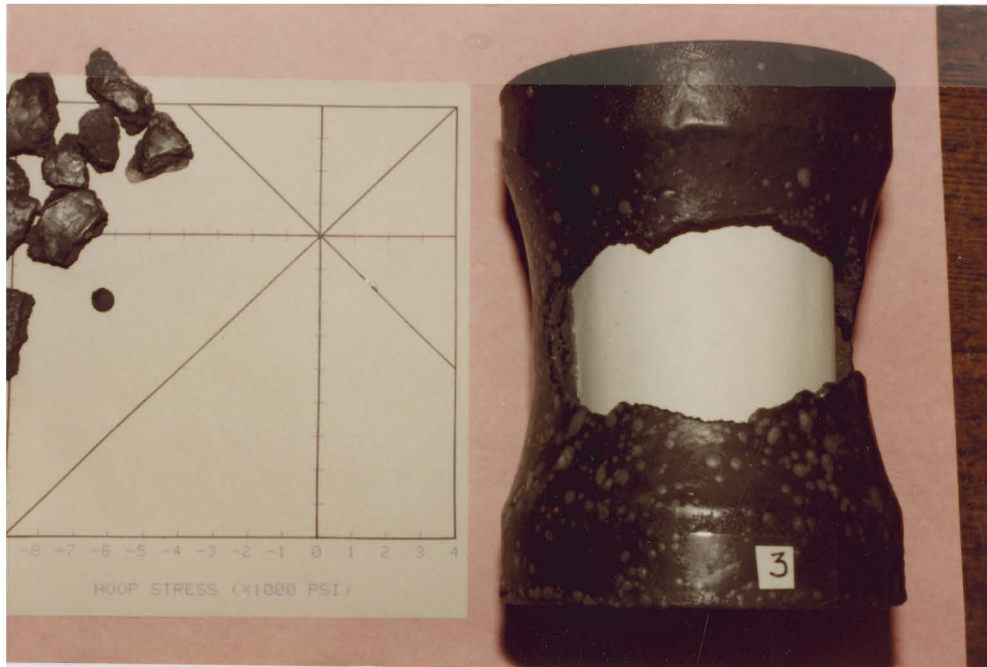
Table 2: Biaxial Test Results (continued)
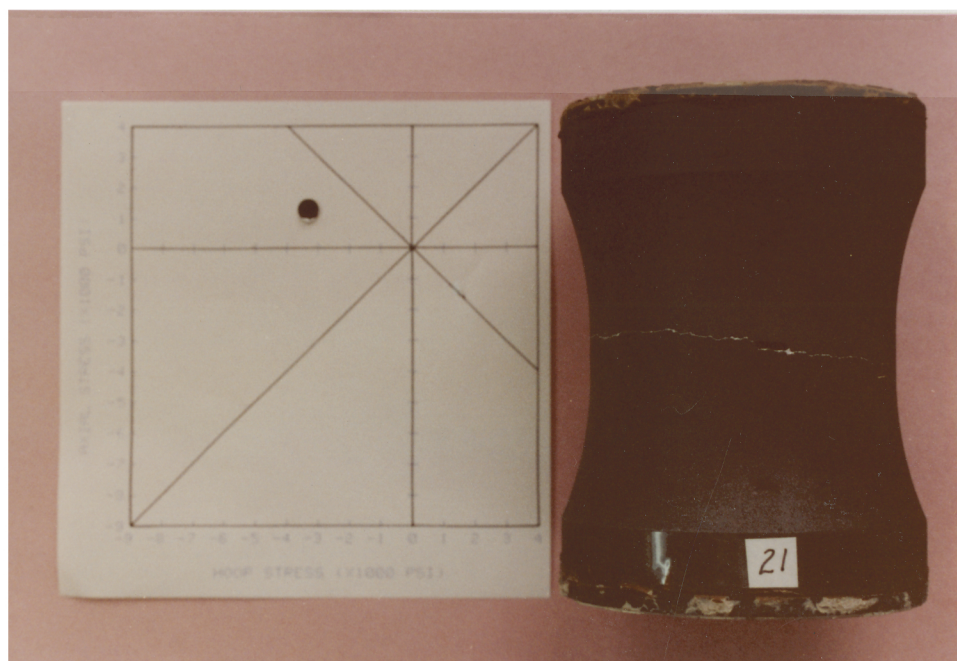
Figure 10(a): Typical C-C Failure Mode

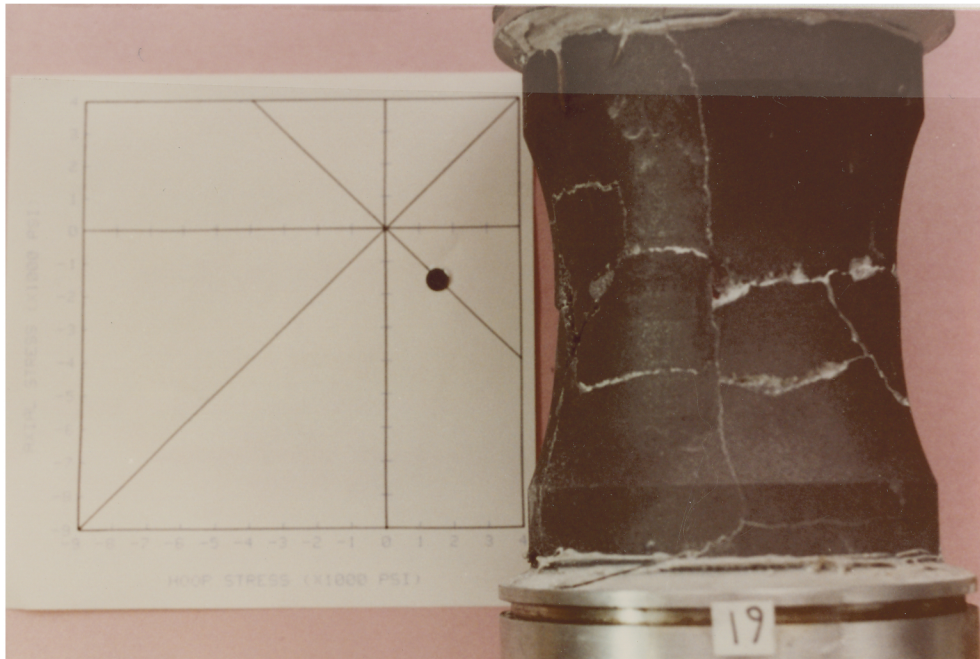Figure 10(b): Typical C-T Failure Mode
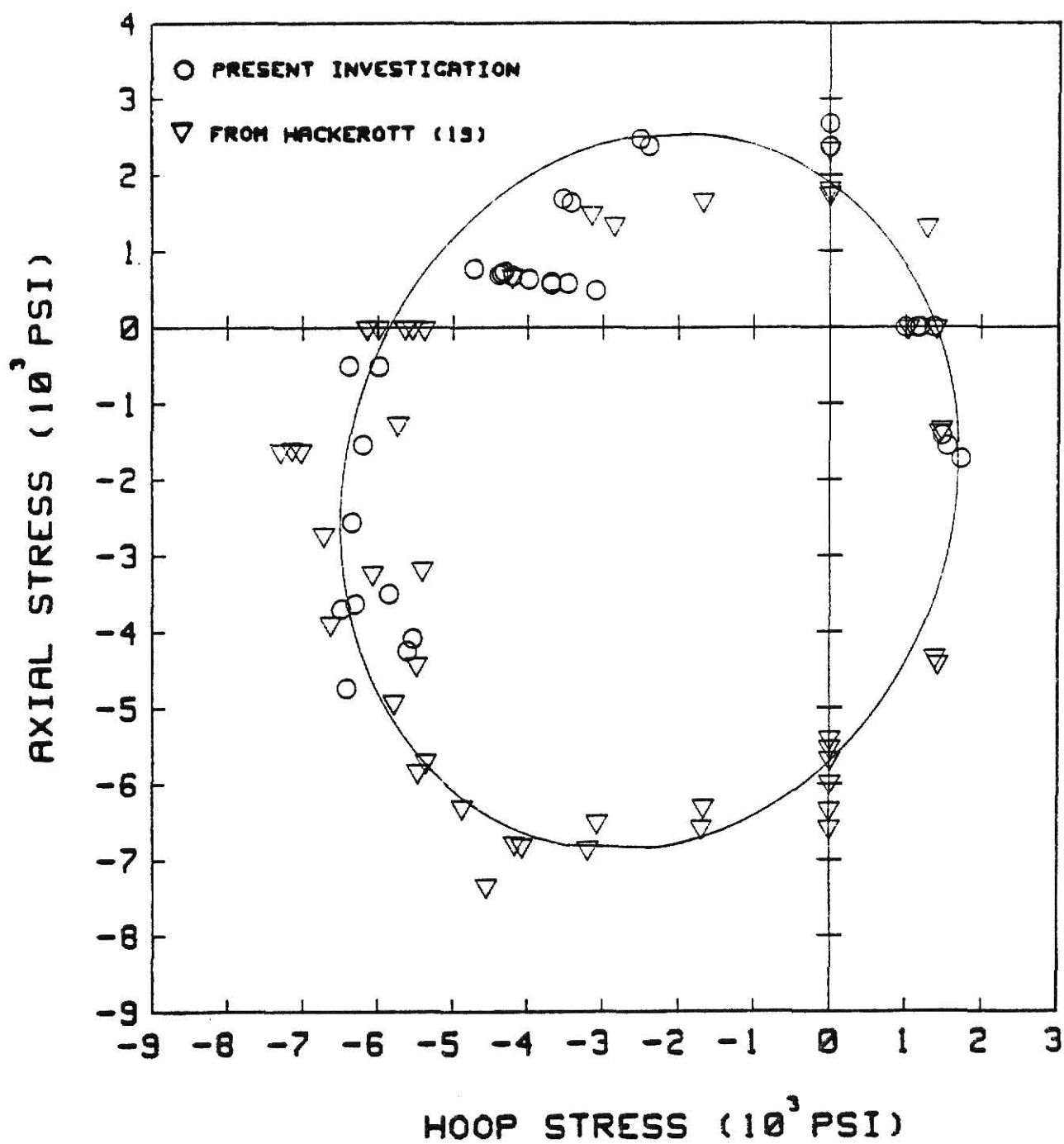
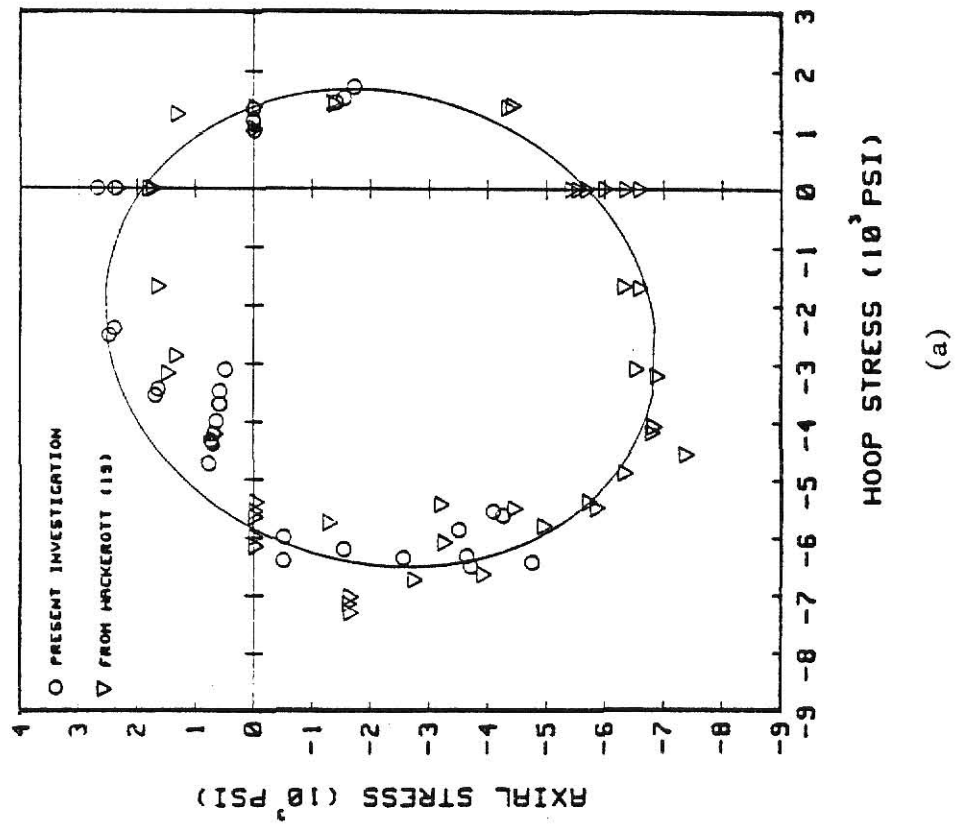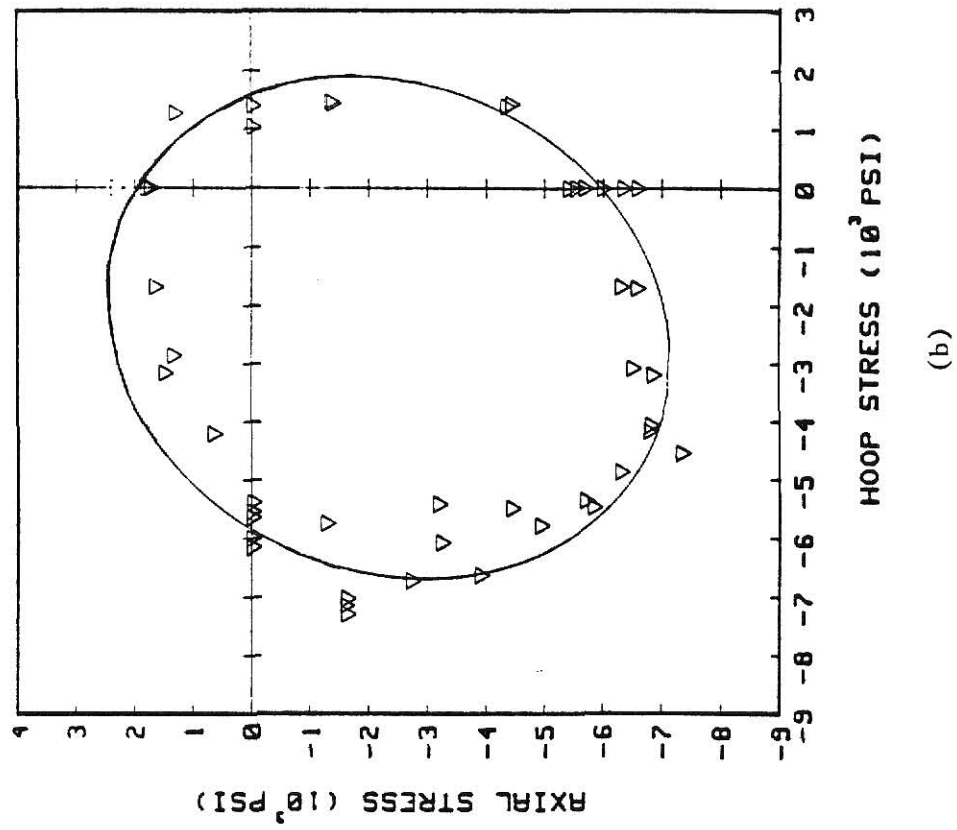Figure 10(c): Typical T-C Failure Mode

Figure 11(a):   Fracture Strength Results

Figure 11: Fracture Strength Results

characterize the failure of graphite. This data exhibits little scatter
while data in the upper portion of the quadrant does exhibit scatter. It
is for this reason that the present investigation has performed additional
biaxial fracture tests in the upper portion of the C-C quadrant using a
different test specimen geometry than that previously used.

Tests 5, 6, 7, 8, 9, and 10 provide data in an area where data pre-
sented by Hackerott exhibited a certain degree of scatter. Tests 5, 6,
and 7 were along a radial line of slope 0.75. Tests 8, 9, and 10 were on
the radial line of slope 0.57. Tests 5 and 6 were very close to one another,
but had slightly low values of strength. Test 7 was a good representation
of the proposed failure surface. There was little scatter between tests
8, 9, and 10 as these points well typified the failure surface.

Other tests were done in the upper portion of the C-C quadrant. Tests
1, 2, 3, and 4 gave good results and fell very close to the proposed fail-
ure surface. Despite the number of additional tests performed in the C-C
quadrant, there was not enough data to statistically represent fracture
strengths along radial lines in the quadrant.

As a whole, biaxial test results obtained in the upper portion of the
C-C quadrant exhibited limited scatter and provided a good fit to the pro-
posed failure surface. Hackerott (19) felt that the data he obtained in
the C-C quadrant, was still influenced by buckling, although not as sig-
nificantly as in other investigations (3, 48). It is hard to determine
whether or not buckling still persists in the present investigation. Better
fit of C-C data to the failure surface, along with the decrease in the de-
gree of data scatter, may indicate a lessening of buckling effects in this
investigation. This lessening of buckling effects has been achieved by use
of a more optimal tubular geometry which is characterized by a shorter gage

length and a thinner wall in the gage section. This specimen geometry not only is more resistant to tubular buckling, but also provides a more uniform stress distribution throughout the wall thickness.

A typical failure mode for C-C fracture tests is shown in Figure 10(a). All C-C test specimens had this type of "hole" fracture. Despite the amount of attention given to the manufacturing of the test specimens, it is often times difficult to do precision machining on graphite. This is due to the amount of tool wear associated with such abrasive machining. It is thought that the "hole" type failure was the result of some unevennes in applying the axial compressive load such that the centerline of the test specimen was not coincident with the centerline of the stainless steel cylinder. Use of teflon pads at the ends of the test specimen allowed for the dissipation of any Poisson's effects at the ends. This helped ensure that failure of the graphite specimens was not initiated by any lateral stresses due to friction acting at the ends.

2) <u>Compression-Tension</u> <u>Tests</u>. Existing biaxial fracture data for EGCR-type AGOT graphite in the compression-tension quadrant previous to this investigation, is very limited. The main emphasis of Hackerott's investigation (19) was to better characterize graphite in the biaxial compression quadrant. In that investigation, Hackerott only tested four specimens in the C-T quadrant. The limited testing in the C-T quadrant was performed in an effort to help provide a better fit of the C-C data to the proposed failure criteria. Biaxial C-T data obtained in this investigation are shown in Figures 8 and 11(a).

Tests 11, 12, 13, 14, 22, 23, 24, 25, 26, 27, and 28 provided confirmation of datum point 47. Loading rates of these specimens were comparable to the rates used by Hackerott, as was mentioned in Chapter III. Results of

these tests help to better define the fracture along a radial line of slope -0.16 in the C-T quadrant.

Biaxial C-T fracture tests 20 and 21 provide added definition to data points 48 and 58 along the radial line of slope -0.48. There is little scatter among the four points even though points 20 and 21 provide a better fit to the failure surface. Incremental loading rates applied to specimens 20, and 21 were smaller than those employed in tests along slope -0.16. Careful attention was given to the pressurization of the test specimens so as to avoid any pressure surges. Such pressure surges are sure to give misleading results because it provides dynamic loading of the test specimens, not static loading. As is the case of all testing done in this investigation, there was not enough data to statistically represent fracture strengths along radial lines in each quadrant.

Tests 15 and 16 provide a significant improvement to datum point 59 along radial line of slope -1.00 (the C-T 45° diagonal, a case of pure shear). There is little scatter between points 15 and 16. Also, these two points better represent the proposed failure surface along the 45° radial line. The incremental loading rate used on the two tests was lower than the loading rates used in all other C-T testing. Again, special attention was given to the loading of the test specimens so as to alleviate any pressure surges in loading.

A typical failure mode for C-T fracture tests is shown in Figure 10(b). The fracture of C-T specimens was a single circumferential crack passing through the gage section. There was no failure at the adhesive bond as noted by Hackerott (19). This may be attributed to the preparation and application of adhesive to the test specimens and allowing for a longer adhesive curing time (at least four days). No failure at the adhesive bond

also indicates that there were, in fact, no significant lateral stresses acting at the specimen ends which initiated failure.

Ho (20), in his biaxial stress tests of graphite, used a tubular specimen geometry with a slenderness ratio four times as large as that used by Hackerott. Although the biaxial tubular geometry used in this investigation was designed with C-C testing in mind, the improved C-T results indicate that the specimen geometry is also good in C-T testing.

3) Tension-Compression Tests. The amount of biaxial fracture test data obtained by Hackerott (19) in the T-C quadrant was also very limited with only four tests made in this quadrant as shown in Figures 7 and 11(b). The limited amount of testing in this quadrant was performed in an effort to help provide a better fit of the C-C data to the proposed failure criteria. Points 42 and 45 exhibit little scatter along radial line of slope -1.00, as do points 46 and 49 along the radial line of slope -3.10. Points 42 and 45 appear to be low in comparison to the proposed failure surface, while points 46 and 49 provide a good fit to the failure criteria.

Figures 7, 8, and 11(a) show that tests 17, 18, and 19 provide confirmation of points 42 and 45. While there is little scatter between this data, point 19 seems to better characterize the failure criteria along the 45° line. Incremental loading rates used on these tests were comparable to tests 20 and 21. Limited testing in this quadrant was done in an effort to provide a better fit of C-C data to the proposed failure criteria.

A typical T-C failure mode is shown in Figure 10(c). Failure of T-C specimens consisted of: A) longitudinal cracks randomly aligned around the specimen, B) horizontal cracks near the bonding, and C) horizontal cracks (generally speaking) in the transitional area between the gage section and the "neck-down" section. The horizontal cracks near the adhesive bond may

indicate that high lateral stresses existed at the specimen ends. Because of the biaxial test method and apparatus, there was no way to tell which type of crack pattern appeared first.

Specimen geometry used in T-C testing is thought to be good even though it was designed with C-C testing in mind. Tests 17, 18, and 19 provide good correlation to the failure surface. Although there may, in fact, be persistant buckling of tubular specimens in the T-C quadrant, it is thought that the geometry used in the present investigation is more resistant to buckling than those used in previous investigations.

Summary of Uniaxial Tensile and Biaxial Fracture Tests

Summary of uniaxial tensile testing and biaxial fracture testing for EGCR-type AGOT graphite are as follows:

1) Uniaxial tensile strength data in the hoop and axial stress directions agree well with data reported in the previous investigation (19) and better characterize the uniaxial tensile strength of the graphite along each coordinate axis.

2) The biaxial test specimen geometry used in this investigation represents a more optimum geometry because of the shorter gage length and the thinner wall thickness.

   a) Less scatter of C-C data in this investigation indicates that the specimen geometry is more resistant to tubular buckling.

   b) A thinner cylinder wall thickness assumes a more uniform stress distribution throughout the wall thickness. An original assumption that allowed us to use the thin-wall equation in calculating hoop stress.

c) This tubular geometry is good for testing graphite in the C-T, and T-C quadrants.

3) C-C data obtained in the upper portion of the quadrant, better characterize the proposed failure surface in that region.

4) Improved values of fracture strength in the C-T quadrant were attained by using smaller loading increments.

5) Fracture strength values along the 45° diagonal in the C-T and T-C quadrants, show an increased improvement over values obtained in the previous investigation (19). These values appear to be more representative of the proposed failure surface.

6) Biaxial fracture strength values obtained along the 45° diagonal in the C-T and T-C quadrants, may now be used to calculate an improved value of the polynomial coefficient F_{13}. Use of this coefficient yields a better fit of the data to the biaxial failure surface.

Comparison of Results with Previous Investigation

Table 3 shows the calculated coefficients of the strength polynomial which were used to find the biaxial failure surface. Uniaxial and biaxial fracture strengths used in evaluating the coefficients are also shown. Results from Hackerott (19) are reproduced for purposes of comparison. The value of X_c used in this investigation is the same as that used by Hackerott (19) and was found by taking the average of uniaxial hoop compression tests. Other values of uniaxial stress were obtained by taking a weighted average of test results along each appropriate coordinate axis.

Figure Number	X_c (psi)	X_t (psi)	Z_c (psi)	Z_t (psi)	σ_3 (psi)	σ_3 (psi)	R_c (psi)	R_t (psi)	F_1 (psi)	F_3 (psi)	F_{11} (psi)	F_{33} (psi)	F_{13} (psi)
11(a)	5849	1400	5700	1900	----	----	2450	1740	5.433×10^{-4}	3.509×10^{-4}	1.221×10^{-7}	9.234×10^{-8}	-1.006×10^{-8}
11(b)	5849*	1600*	5957*	1974*	-6300*	-4868*	----	----	$4.538* \times 10^{-4}$	$3.387* \times 10^{-4}$	$1.070* \times 10^{-7}$	$8.504* \times 10^{-8}$	$-1.229* \times 10^{-8}$

*from (19)

Table 3: Uniaxial and Biaxial Fracture Strengths with Calculated Polynomial Coefficients

Figure 11(a) shows the failure surface in biaxial stress space as calculated using the polynomial coefficients of Table 3. For purposes of comparison, the failure surface presented by Hackerott (19) is shown in Figure 11(b).

The failure surface presented by Hackerott was found using a value of F_{13} which was based on biaxial C-C data as shown by Equation (8). Biaxial data along the 45° diagonal in the C-T and T-C quadrants were not used by Hackerott to find F_{13}. This was done because of the limited amount of biaxial data obtained along the 45° diagonal. It is also noteworthy that the choice of the C-C datum point is very arbitrary and is left to the discretion of the investigator.

The value of F_{13} in this investigation can be calculated very easily by use of uniaxial data, along with biaxial fracture data obtained along the 45° diagonal in the C-T and T-C quadrants as shown by Equation (7). For these reasons, it is felt that the failure surface of Figure 11(a) better characterizes the fracture strength of EGCR-type grade-AGOT graphite.

CHAPTER V

LITERATURE REVIEW OF POLYAXIAL TEST METHODS

Introduction

To completely characterize transversely isotropic AGOT graphite, it is
necessary to evaluate the seven strength constants F_i, F_3, F_{11}, F_{33}, F_{44},
F_{12}, and F_{13}. Constants F_1, F_3, F_{11}, F_{33}, and F_{13} may be obtained by uni-
axial and biaxial tests as was done in Chapter III of this investigation.
Constants F_{44} and F_{12} must be obtained by way of a polyaxial test--polyaxial
in the sense that $\sigma_1 \neq \sigma_2 \neq \sigma_3$. Prior to this investigation, such a polyaxial
test program of graphite was considered by the author. For this reason, a
literature review of existing polyaxial test methods for brittle materials
was undertaken. The results of the literature review are, hence, included
and are described by the type of test specimen employed. References are
also given so as to facilitate any future work towards the polyaxial testing
of AGOT graphite.

Solid Cylinder

Testing of solid cylinder specimens was usually done by applying an
axial compressive load at the specimen ends while applying hydrostatic pres-
sure to the outside of the cylinder. Although it is often times referred to
as polyaxial, this test method only has two independent stresses, e.g.
$\sigma_1 \neq \sigma_2 = \sigma_3$. References pertaining to this type of triaxial testing are as

follows:

1. Newman, J. B., "Apparatus for Testing Concrete under Multiaxial States of Stress," Magazine of Concrete Research, Vol. 26, No. 89, December 1974, pp. 229-238.

2. Ehrenburg, D.O., "Fracture Criteria for Brittle Materials," Journal of Testing and Evaluation, Vol. 4, No. 3, May 1976, pp. 200-208.

3. Meerman, W.C.P.M., A.C. Knappan, "A High-Pressure Triaxial Testing Cell", Powder Technology, Vol. 22, No. 2, March-April 1979, pp. 271-278.

4. Gerstle, K.H. and others, "Behavior of Concrete under Multiaxial Stress States", Journal of Engineering Mechanics Division, Proceedings of the American Society of Civil Engineers, Vol. 106, No. EM6, December 1980, pp. 1383-1403.

Hollow Cylinders

There has been widespread use of hollow cylinder test specimens in the testing of brittle materials. Many different specimen geometries and end conditions have been used. States of stress are achieved by pressurizing the cylinder ends, along with the inside and outside cylinder walls. As is the case of the solid cylinder test specimen, this type of testing has only two independent stresses, e.g. $\sigma_1 \neq \sigma_2 = \sigma_3$. References representative of this type of triaxial testing are:

5. Broutman, L. J., S.M. Krishnakumar, and P.K. Mallick, "Effects of Combined Stresses on Fracture of Alumina and Graphite", J. American Ceramic Society, 53, 1970, p. 649.

6. Weng, T., "Structural and Physical Properties of Graphite-Zirconium Diboride-Silicon Carbide Composites", Technical Report AFML-TR-70-50, May 1970, Union Carbide Corporation, Carbon Products Division, pp. 31-33.

7. Babcock, S.G., S.J. Green, P.A. Hochstein, and J.A. Gum, "Dynamic Biaxial and Elevated-Temperature Properties of ATJ-S Graphite", Proceedings of the Conference on Continuum Aspects of Graphite Design, November 9-12, 1970, Gatlinburg, Tennessee, CONF-701105, NTIS, U.S. Department of Commerce, pp. 50-59.

8. Jortner, J., "Biaxial Mechanical Properties of AXF-5Q Graphite to 4000°F", <u>Proceedings of the Conference on Continuum Aspects of Graphite Design</u>, November 9-12, 1970, Gatlinburg, Tennessee, CONF-701105.

9. Weng, T., "Stress-Strain Properties of Grade ATJ Graphite Under Combined Stresses", <u>Proceedings of the Conference on Continuum Aspects of Graphite Design</u>, November 9-12, 1970, Gatlinburg, Tennessee, CONF-701105, NTIS, U.S. Department of Commerce, pp. 222-235.

10. Jortner, J., "Multiaxial Behavior of ATJ-S Graphite", Technical Report AFML-TR-71-253, December 1971.

11. Ely, R.E., "Strength Results for Two Brittle Materials Under Biaxial Stresses", Report RR-TR-72-11, 1972, U.S. Army Missiles Command, Redstone Arsenal, AL.

12. Greenstreet, W.L., B.Y. Yahr, and R.S. Valachovic, "Fracture of Graphite", ORNL-TM-3936, Oak Ridge National Lab., Oak Ridge, Tennessee, October 1972.

13. Jortner, J., "Multiaxial Response of ATJ-S Graphite", Technical Report AFML-TR-73-170, October 1973.

14. Hackerott, H.A., "Characterization of Multiaxial Fracture Strength of Transversely Isotropic AGOT Graphite", M.S. Thesis, Kansas State University, 1982.

Cubic

Recent triaxial tests of brittle materials have employed the cubic shaped test specimen. This test method has a distinct advantage over the previously mentioned method because it is capable of inducing pure polyaxial stresses on the test specimen, e.g. $\sigma_1 \neq \sigma_2 \neq \sigma_3$. References pertaining to this type of testing are as follows:

15. Gerstle, K.H., "Behavior of Concrete under Multiaxial Stress States", <u>Journal of the Engineering Mechanics Division, Proceedings of the American Society of Civil Engineers</u>, Vol. 106, No. EM6, December 1980.

16. Atkinson, R.H., "A Cubical Test Cell for Multiaxial Testing of Materials", Ph.D. Thesis, University of Colorado, 1972.

17. Sture, S., "An Improved Multiaxial Cubical Cell and Its Applica-
     tion to the Testing of Anisotropic Materials", M.S. Thesis,
     University of Colorado, 1973.

18. Atkinson, R.H., H.Y. Ko, "A Fluid Cushion Multiaxial Cell for
     Testing of Cubical Rock Specimens", <u>International Journal of Rock
     Mechanics and Mining Science and Geomechanics</u>, Vol. 10, 1973,
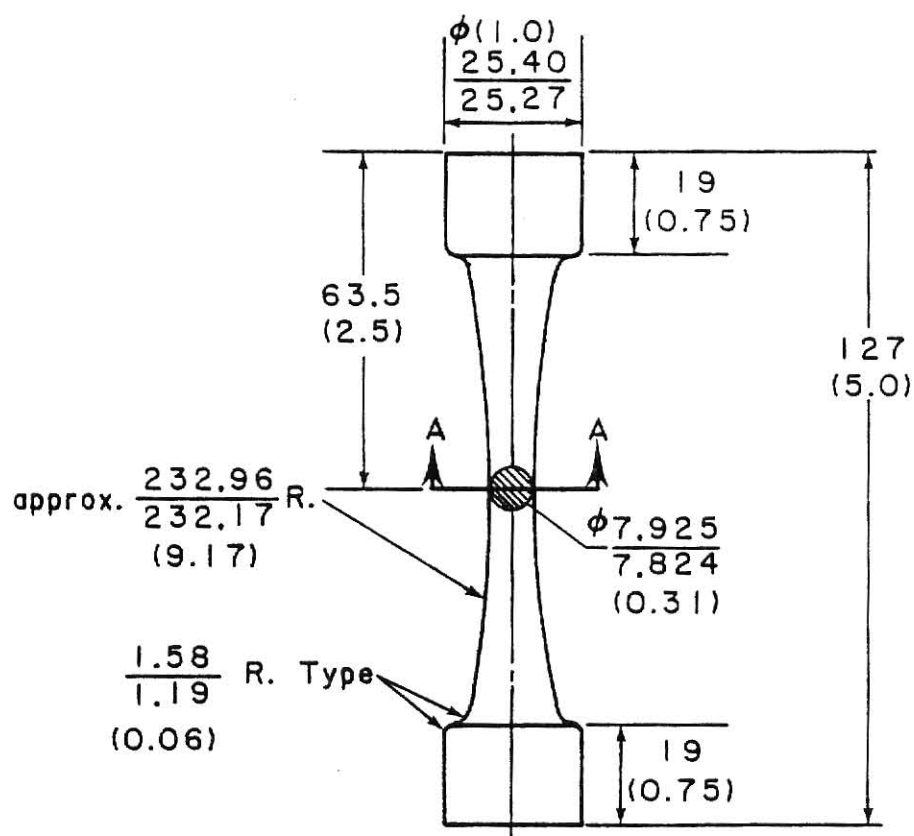   pp. 351-361.

BIBLIOGRAPHY

1. Babcock, S.G., S.J. Green, P.A. Hochstein, and J.A. Gum, "Dynamic Biaxial and Elevated-Temperature Properties of ATJ-S Graphite", <u>Proceedings of the Conference on Continuum Aspects of Graphite Design</u>, November 9-12, 1970, Gatlinburg, Tennessee, CONF-701105, NTIS. U.S. Department of Commerce, p. 50-59.

2. Broutman, L.J., S.M. Krishnakumar, and P.K. Mallick, "Effects of Combined Stresses on Fracture of Alumina and Graphite", <u>J. American Ceramic Society</u>, 53, 1970, p. 649.

3. Chang, T.Y. and T. Weng, "A Strength Criterion for Graphite Under Combined Stress", ASME PVP Meeting, June 1975.

4. Cobb, H. R. W., S. J. S. Parry, and G. B. Engle, "Characterization of Production-Grade H-327 Graphite for HTER Design", <u>Proceedings of the Conference on Conuinuum Aspects of Graphite Design</u>, November 9-12, 1970, Gatlinburg, Tennessee, CONF-701105, NTIS, U.S. Department of Commerce, pp. 98-114.

5. Coffin, L.F., Jr., "The flow and Fracture of a Brittle Material", <u>Journal of Applied Mechanics</u>, Trans. ASME, Vol. 72, September 1950, pp. 233-248.

6. Coulomb, C.A., "Memoires de Mathematique et de Physique", <u>Academie Royal des Sciences par divers savants</u>, Vol. 7, 1773, p. 343.

7. Ely, R.E., "Strength of Graphite Tube Specimens Under Combined Stress", <u>J. American Ceramic Society</u>, 48 (10), 1965, pp. 505-508.

8. Ely, R.E., "Biaxial Fracture Stress for Graphite, Ceramic and Filled and Reinforced Epoxy Tube Specimens", Report RR-TR-65-10, June 1965, U.S. Army Missles Command, Redstone Arsenal, Alabama.

9. Ely, E., "Strength of Magnesium Silicate and Graphite Under Biaxial Stresses", <u>Ceramic Bulletin</u>, Vol. 47, No. 5, 1968, pp. 489-492.

10. Ely, R.E., "Strength Results for Ceramic Materials Under Multiaxial Stresses", U.S. Army Missile Command Report RR-TR-68-1, April 1968.

11. Ely, R.E., "Strength Results for Two Brittle Materials Under Biaxial Stresses", Report RR-TR-72-11, 1972, U.S. Army Missle Command, Redstone Arsenal, Alabama.

12. Ely, R.E., "Strength Results for Two Brittle Materials Under Biaxial Stresses", Report RR-TR-72-11, 1972, U.S. Army Missiles Command, Redstone Arsenal, Alabama.

13. Fisher, J.C., "A Criterion for the Failure of Cast Iron", <u>ASTM Bulletin</u>, No. 181, April 1952, pp. 74-75.

14. Gol'denblat, I.I. and V.A. Kopnov, "Strength of Glass-Reinforced Plastics in the Complex Stress State", Mekhanika Polimerov, Vol. 1, 1965, p. 70; English Translation: Polymer Mechanics, Vol. 1, 1966, p. 54. Faraday Press.

15. Grassi, R.C. and I., Cornet, "Fracture of Gray Cast-Iron Tubes Under Biaxial Stresses", Mechanical Engineering, Vol. 70, 1948, p. 918.

16. Greenstreet, W.L., J.E. Smith, and G.T. Yahr, "Mechanical Properties of EGCR-type AGOT Graphite," Carbon, Vol. 7, 1969, pp. 15-45.

17. Greenstreet, W.L., G.Y. Yahr, and R.S. Valachovic, "Fracture of Graphites" ORNL-TM-3936, Oak Ridge National Lab., Oak Ridge, Tennessee, October 1972.

18. Greenstreet, W.L., G.T. Yahr, and R.S. Valachovic, "The Behavior of Graphite under Biaxial Tension", Carbon, Vol. 11, 1973, pp. 43-57.

19. Hackerott, H.A., "Characterization of Multiaxial Fracture Strength of Transversely Isotropic AGOT Graphite", M.S. Thesis, Kansas State University, 1982.

20. Ho, F., "Specification for Biaxial Stress Test", GA Document No. 902984, April 20, 1977.

21. Hoffman, O., "The Brittle Strength of Orthotropic Materials", J. of Composite Materials, Vol. 1, No. 2, April 1967, pp. 200-205.

22. Huang, C.L., "On Quadratic Strength Function for Anisotropic Materials", Proceedings of the 1974 Symposium on Mech. Behavior of Materials, Kyoto, Japan, 1974.

23. Huang, C.L., "On Strength Function for Anisotropic Materials", Proceedings of Symmetry, Similarity and Group-Theoretic Methods in Mechanics, The University of Calgary, Canada, 1974.

24. Huang, C.L. and P.G. Kirmser, "A Criterion of Strength for Orthotropic Materials", Fibre Science Technology, Vol. 8, 1975, pp. 103-112.

25. Jortner, J., "Biaxial Mechanical Properties of AXF-5Q Graphite to 4000°F", Proceedings of the Conference on Continuum Aspects of Graphite Design, November 9-12, 1970, Gatlinburg, Tennessee, CONF-701105.

26. Jortner, J., "Multiaxial Behavior of ATJ-S Graphite", Technical Report AFML-TR-71-160, July 1971.

27. Jortner, J., "Multiaxial Behavior of ATJ-S Graphite", Technical Report AFML-TR-71-253, December 1971.

28. Jortner, J., "Multiaxial Response of ATJ-S Graphite", Technical Report AFML-TR-73-170, October 1973.
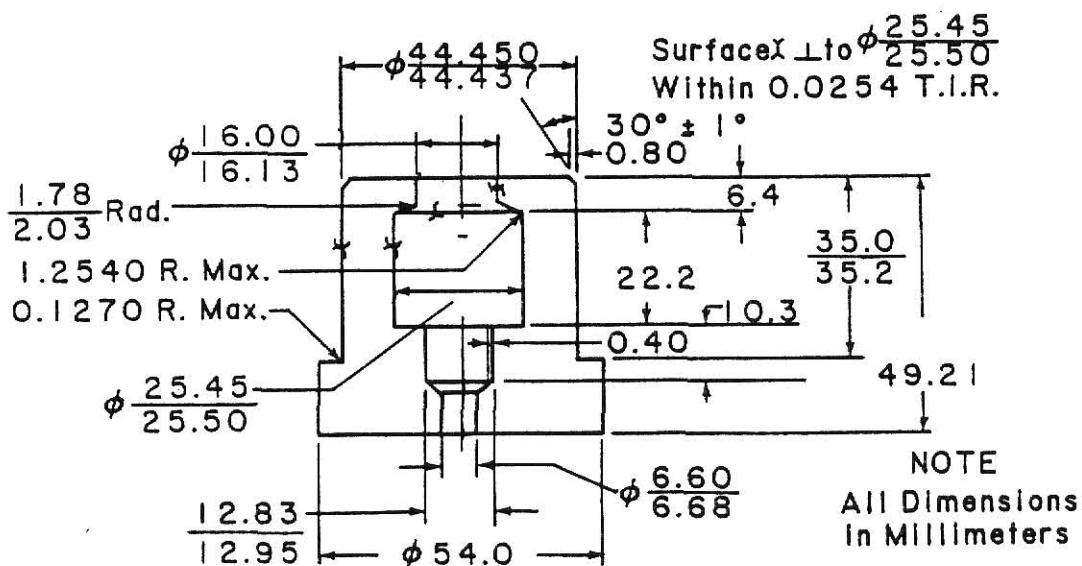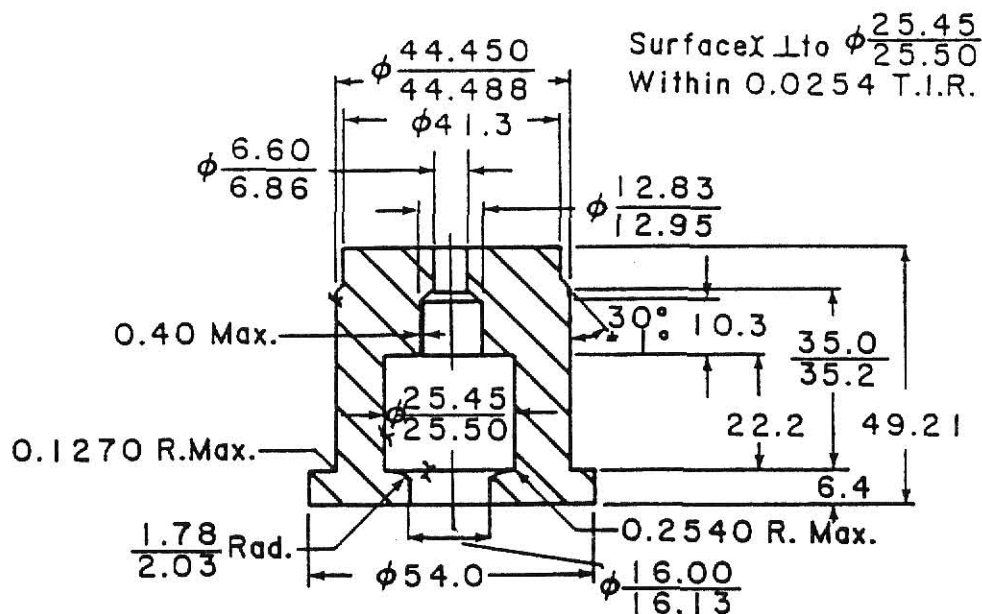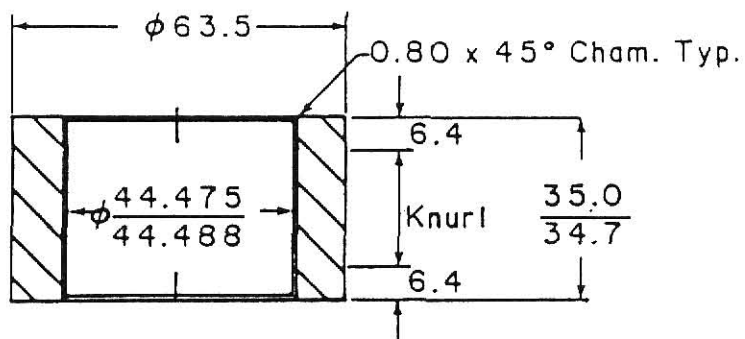
29. Knibbs, R.H., "Fracture of Polycrystalline Graphite", J. Nucl. Mat., Vol. 24, 1967, pp. 174-187.

30. Marshall, P. and E.K. Priddle, "The Influence of Specimen Size and Mode of Loading on the Fracture of Graphite", Carbon, Vol. 11, 1973, pp. 627-631.

31. Merkle, J.G., "An Ellipsoidal Yield Function for Materials that can Both Dilate and Compact Inelastically," Nuclear Engineering and Design, 12, 1970, pp. 425-451.

32. Mises, R. Von, "Mechanik der Festen Koerper im Plastischen Deformable Zustand", Nachrichten der Gesellschaft der Wissenschaften Goettingen, Mathematisch-Physisch Klasse, Goettingen, 1913.

33. Mohr, O., "Welche Umstände bedingen die Elästiztatsgrenze und den Bruch eines Materials?", Zeitchrift des Vereines Deutscher Ingenieure, Vo. 44, 1900, p. 1524.

34. Nightingale, R.E., ed., Nuclear Graphite, Academic Press, 1962.

35. Paul, B., "A Modification of the Coulomb-Mohr Theory of Fracture", J. of Applied Mechanics, Vol. 28, 1961, p. 259.

36. Paul, B., "Generalized Pyramidal Fracture and Yield Criteria", Int. J. Solids and Structures, Vol. 4, 1968, p. 175.

37. Paul, B., "Macroscopic Criteria for Plastic Flow and Brittle Fracture", Ch. 4, Vol. II, Fracture, An Advanced Treatise, Academic Press, 1968.

38. Peng, S.D., "Fracture and Failure of Chelmsford Granite", p. 323, Ph.D. Thesis, Stanford University, 1970.

39. Peng, S.D., "Stresses Within Elastic Circular Cylinders Loaded Uni-axially and Triaxially", Int. J. Rock Mech. Min. Sci., Vol. I, Pergamon Press 1971, pp. 399-432.

40. Price, R.J., and H.R.W. Cobb, "Application of Weibull Statistical Theory to the Strength of Reactor Graphite", Report GA-10257, Gulf General Atomic Company, August 6, 1970.

41. Price, R.J., "Mechanical Properties of Graphite for High-Temperature Gas-Cooled Reactors: A Review", General Atomic Report GA-A13524, September 22, 1975.

42. Tang, P.Y., "A Recommendation of a Triaxial Failure Theory for Graphite", U.S. Department of Commerce, Department of Commerce, Department of Energy, No. GA-A1533 UC-77, May 1979.

43. Taylor, R., R.G. Brown, K. Gilchrist, E. Hall, A.T. Hodds, B.T. Kelly, and F. Morris, "The Mechanical Properties of Reactor Graphite", Carbon Vol. 5, 1967, pp. 519-531.
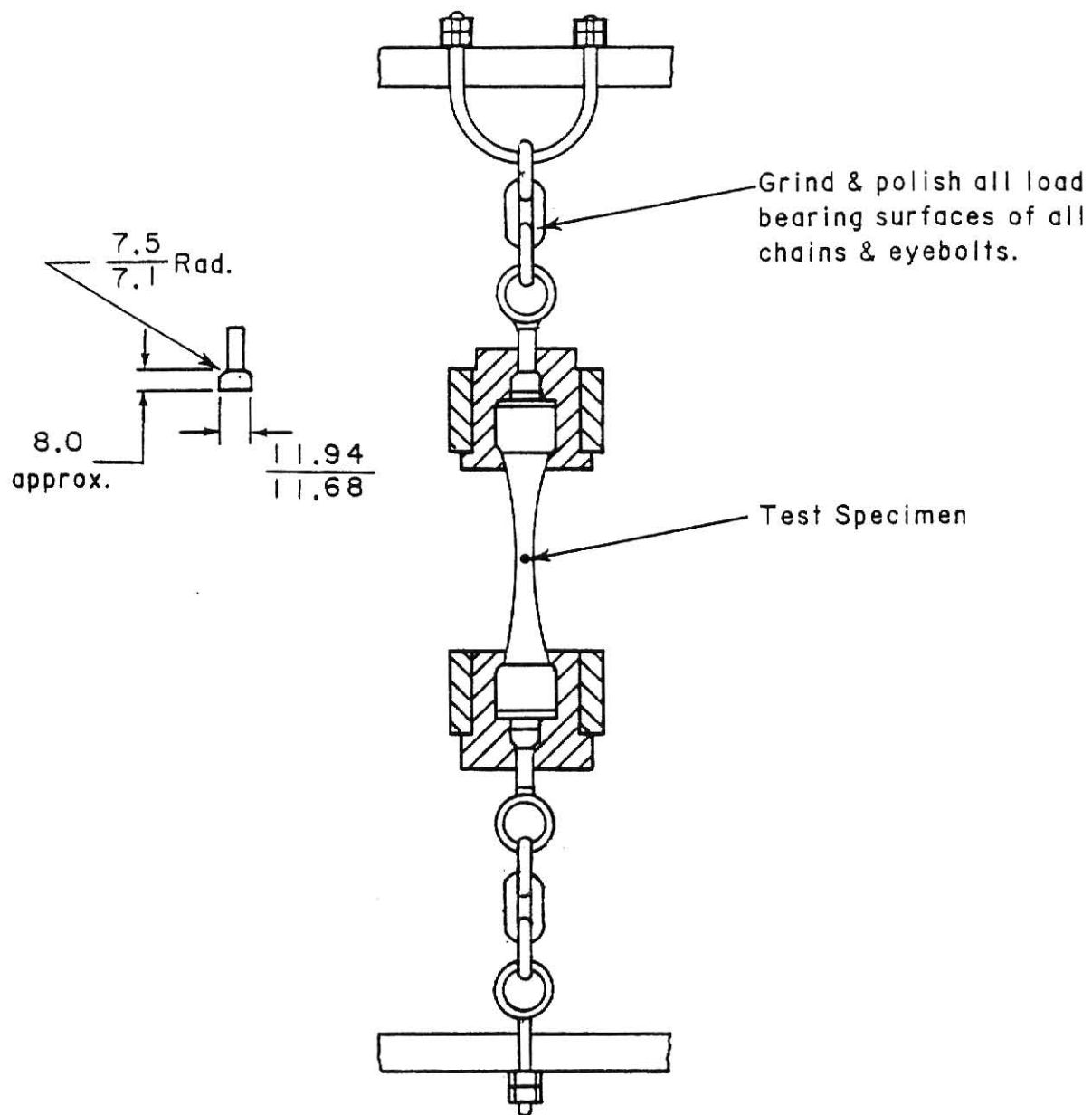
44. Tresca, H., "Sur l' encoulement des corps solides soumis à les fortes pressions", C.R. Hebd. Séanc. Acad. Sci, Paris. 59, 1964, pp. 754-758.

45. Tsai, S.W. and F.M. Wu, "A General Theory of Strength for Anisotropic Materials", Journal of Composite Materials, Vol. 5, January 1971, pp. 58-80.

46. Union Carbide Corporation, The Industrial Graphite Engineering Handbook, Union Carbide Corporation, New York, 1970, p. 5A.05.01.

47. Weng, T., "Room Temperature Fracture Behavior of Polycrystalline Graphite Under Torsional and Biaxial Stresses", Paper No. MI 60, Presented at Eighth Biennial Conference on Carbon, Buffalo, NY, June 19-23. 1967.

48. Weng, T., "Biaxial Fracture Strength and Mechanical Properties of Graphite-Base Refractory Composites", AIAA Journal, Vol. 7, No. 5, May 1969, pp. 851-858.

49. Weng, T., "Structural and Physical Properties of Graphite-Zirconium Diboride-Silicon Carbide Composites", Technical Report AFML-TR-70-50, May 1970, Union Carbide Corporation, Carbon Products Division, pp. 31-33.

50. Weng, T., "Stress-Strain Properties of Grade ATJ Graphite Under Combined Stress", Proceedings of the Conference on Continuum Aspects of Graphite Design, November 9-12, 1970, Gatlinburg, Tennessee, CONF-701105, NTIS, U.S. Department of Commerce, pp. 222-235.

APPENDIX

Reprinted from ASTM Standard C565-78

$\phi 63.5$

−0.80 x 45° Cham. Typ.

6.4

Knurl

$\frac{35.0}{34.7}$

6.4

$\phi \frac{44.475}{44.488}$

$\phi \frac{44.450}{44.488}$

$\phi 41.3$

$\phi \frac{6.60}{6.86}$

$\phi \frac{12.83}{12.95}$

Surface X ⊥ to $\phi \frac{25.45}{25.50}$
Within 0.0254 T.I.R.

30° 10.3

$\frac{35.0}{35.2}$

0.40 Max.

$\phi \frac{25.45}{25.50}$

22.2   49.21

0.1270 R. Max.

6.4

$\frac{1.78}{2.03}$ Rad.

−0.2540 R. Max.

$\phi 54.0$ $\phi \frac{16.00}{16.13}$

$\phi \frac{44.450}{44.437}$

Surface X ⊥ to $\phi \frac{25.45}{25.50}$
Within 0.0254 T.I.R.

30° ± 1°
0.80

$\phi \frac{16.00}{16.13}$

6.4

$\frac{1.78}{2.03}$ Rad.

$\frac{35.0}{35.2}$

1.2540 R. Max.

22.2

0.1270 R. Max.

⌐10.3

0.40

49.21

$\phi \frac{25.45}{25.50}$

$\phi \frac{6.60}{6.68}$

12.83

$\phi 54.0$

12.95

NOTE
All Dimensions
In Millimeters

7.5 / 7.1 Rad.

8.0 approx.

11.94 / 11.68

Grind & polish all load bearing surfaces of all chains & eyebolts.

Test Specimen

VITA

Enrique Samuel Garibay

Candidate for the Degree of

Master of Science

Thesis: <u>An Improved Characterization of the Multiaxial Fracture Strength of EGCR-type AGOT Graphite</u>

Major Field: Mechanical Engineering

Biographical:

Personal Data: Born in Manhattan, Kansas, October 7, 1958, son of Michael and Josephine Garibay.

Education: Received Bachelor of Science degree from Kansas State University, with a major in Mechanical Engineering, in May, 1981.

Professional and
Honorary Organizations: American Society of Mechanical Engineers, American Society of Heating, Refrigerating, and Air Conditioning, MEChA, Society of Ethnic Minority Engineers, "Engineer in Training," certified June 1981.

Professional Experience: Associate Director of Minority Engineering Study Center, Dean of Engineering Kansas State University, August 1981-82; Associate Engineer, Martin-Marietta Aerospace, Denver, Colorado, Summer 1981; Production Engineer, IBM, Boulder, Colorado, Summer 1980; Systems Engineer, IBM, Kansas City, Missouri, Summer 1979; Co-op PBX Engineer, Southwestern Bell, September 1977-September 1978; Welder, M-F Welding, Manhattan, Kansas, Summers 1972-1976.

AN IMPROVED CHARACTERIZATION OF THE MULTIAXIAL
FRACTURE STRENGTH OF EGCR-TYPE AGOT GRAPHITE

by

ENRIQUE SAMUEL GARIBAY

B.S., Kansas State University, 1981

AN ABSTRACT OF A MASTER'S THESIS

submitted in partial fulfillment of the

requirements for the degree

MASTER OF SCIENCE

Department of Mechanical Engineering

KANSAS STATE UNIVERSITY
Manhattan, Kansas

1983

ABSTRACT

Brittle solid materials such as graphite are now being used in many
diverse applications in essentially all of industry. With graphite having
a high strength-to-weight ratio, it has become one of the leading materials
to be used in rockets and missles as unusual cone, nozzle, and vane shapes.
In nuclear applications, graphite is used as a moderator, reflector, ther-
mal column, and a shielding structure because of the increase in strength
and hardness when exposed to irradiation.

The broadening applications of transversely isotropic graphite demon-
strate that it is indeed a versatile industrial material. In order to take
full advantage of its versatility, it is first necessary to characterize
the fracture strength of the material under a combined state of stress.
In this study, the fracture strength of EGCR-type grade-AGOT graphite is
studied in the Compression-Compression, Compression-Tension, and Tension-
Compression quadrants of biaxial stress.

Fracture strength data for EGCR-type grade-AGOT graphite was found by
conducting uniaxial and biaxial fracture tests at room temperature. Uni-
axial tensile tests were conducted in the hoop and axial stress directions
using "dog-bone" shaped test specimens. Biaxial fracture tests were con-
ducted using the "pressure vessel" method. Thin-walled cylinders were sub-
jected to a combination of inside pressure, outside pressure, and an axial
load.

Finding the true fracture strength of brittle materials can often be
complicated and difficult. When thin-walled cylinders are used in biaxial
tests, it is necessary to choose an optimum specimen geometry which will
be resistant to tubular buckling while maintaining a uniform stress

distribution throughout the wall thickness.

Once fracture data has been obtained, it is then necessary to correlate the data to a quadratic polynomial failure theory which describes a ellipsoidal failure surface in biaxial stress space. The failure theory is made up of five independent strength constants which are evaluated by use of uniaxial and biaxial fracture data.

Fracture strength data obtained in this investigation seem to better characterize the failure surface of EGCR-type grade-AGOT graphite. The biaxial fracture strength values along the 45° diagonal in the Compression-Tension and Tension-Compression quadrants show an increased improvement over values obtained in a previous investigation and can now be used to provide a better fit of the fracture data to the proposed biaxial failure surface.